

Quantum geometric contributions to the BKT transition: Beyond mean field theoryZhiqiang Wang ¹, Gaurav Chaudhary ¹, Qijin Chen ², and K. Levin ¹¹*James Franck Institute, University of Chicago, Chicago, Illinois 60637, USA*²*Shanghai Branch, National Laboratory for Physical Sciences at Microscale and Department of Modern Physics, University of Science and Technology of China, Shanghai 201315, China* (Received 3 August 2020; revised 16 October 2020; accepted 20 October 2020; published 4 November 2020)

We study quantum geometric contributions to the Berezinskii-Kosterlitz-Thouless (BKT) transition temperature T_{BKT} in the presence of fluctuations beyond BCS theory. Because quantum geometric effects become progressively more important with stronger pairing attraction, a full understanding of 2D multiorbital superconductivity requires the incorporation of preformed pairs. We find it is through the effective mass of these pairs that quantum geometry enters the theory and this suggests that the quantum geometric effects are present in the nonsuperconducting pseudogap phase as well. Increasing these geometric contributions tends to raise T_{BKT} , which then competes with fluctuation effects that generally depress it. We argue that a way to physically quantify the magnitude of these geometric terms is in terms of the ratio of the pairing onset temperature T^* to T_{BKT} . Our paper calls attention to an experimental study demonstrating how both temperatures and, thus, their ratio may be currently accessible. They can be extracted from the same voltage-current measurements, which are generally used to establish BKT physics. We use these observations to provide rough preliminary estimates of the magnitude of the geometric contributions in, for example, magic angle twisted bilayer graphene.

DOI: [10.1103/PhysRevB.102.184504](https://doi.org/10.1103/PhysRevB.102.184504)**I. INTRODUCTION**

The recent discovery of superconducting phases in twisted bilayer graphene (TBLG) at the first magic angle has attracted much attention [1–15]. The excitement surrounding this material is driven largely by the flatness of the energy bands, which effectively enhances the importance of electron-electron interactions. This stronger interaction effect is consistent with the observed high superconducting transition temperatures [2] and has been speculated to place TBLG somewhere in the crossover between the BCS and the Bose-Einstein condensation (BEC) regimes [2,16,17]. Because of its two dimensionality (2D) this superconductivity is associated with a BKT instability, in which the transition temperature T_{BKT} is directly proportional to the superfluid phase stiffness [18–20]. In a single flat band, this stiffness vanishes; however, in multiorbital band models, it was shown that the inclusion of quantum geometric effects may reinstate a finite transition temperature [21–25].

This physical picture of flat-band superconductivity has been established within BCS mean field (MF) theory, which is known to be problematic in 2D. Moreover, quantum geometric effects become most apparent outside the BCS regime, where noncondensed pairs, neglected in MF theory, play an important role in the phase stiffness.

In this paper, we present a theory which addresses these shortcomings through studies of the interplay of preformed pairs with quantum geometric effects. We determine T_{BKT} , in 2D superconductors using a simple two-band tight-binding model [26,27] that captures some key ingredients in common with its TBLG counterpart, including potentially nontrivial

band topology. The model has some formal similarities to a spin-orbit coupled Fermi gas Hamiltonian, where the nature of (albeit, three dimensional) pairing fluctuations within the BCS-BEC crossover is well studied [28–32]. Built on the BCS-Leggett ground state [33], our approach yields results for T_{BKT} that are consistent with the mean field literature at weak attraction, precisely where the MF theory is expected to work.

A major contribution of this paper is to establish the important competition: bosonic excitations lead to a decrease in the effective phase stiffness, whereas, geometric effects generally cause an increase. These latter become more appreciable as the bands become flatter. As a result, T_{BKT} remains substantial, even though it is reduced by beyond mean field fluctuations. An important finding is that geometric contributions appear through the inverse pair mass, $1/M_{\text{B}}$. Unlike in previous work [34,35] where the pair mass was also found to depend on quantum geometry, here M_{B} incorporates the self-consistently determined pairing gap. Because M_{B} enters the excitation spectrum of the pairs, the effect of geometry must be present in a host of general characteristics beyond the superfluid stiffness including transport and thermodynamics [36], persisting even into the pseudogap phase. Here the “pseudogap phase” refers to the nonsuperconducting state with preformed pairs at $T_{\text{BKT}} < T < T^*$. We reserve the term “normal state” for a noninteracting system without pairing.

To physically understand the relation between the pair mass and geometry, note that an increased magnitude of the quantum metric reflects an increased spatial extent of the normal state Wannier orbitals [37,38]. This increase leads to larger pairs, which have a bigger overlap, leading to higher

pair mobility (smaller M_B). Nontrivial normal state band topology enhances these effects, which become most apparent in the so-called “isolated flat band limit” [22], where the conventional contributions to the pair mobility are negligible. In analogy with earlier findings [21,22], we demonstrate that a nontrivial band topology provides a lower bound for $1/M_B$ in this limit.

Finally, it is important to determine the size of the geometric contributions using experimentally accessible quantities. We find that the ratio of the pairing onset temperature T^* and T_{BKT} allows quantification of the geometric contributions and characterization of a given 2D superconductor more generally. We demonstrate how both temperatures can be determined from the same voltage-current measurements [39].

The rest of the paper is organized as follows. Section II introduces the theoretical approach for deriving the BKT transition temperature. This includes the introduction of the topological band model, our pairing fluctuation theory and a procedure for calculating the transition temperature as approached from the nonsuperconducting state. We also present a discussion of the isolated flat band limit where we derive a lower bound for n_B/M_B associated with band topology. Here n_B is the areal density of preformed pairs. The corresponding numerical results for T_{BKT} and T^* are presented in Sec. III. Based on our numerical results and an experimental estimate of T^*/T_{BKT} , we speculate that magic angle TBLG is in the BCS-BEC crossover regime, although it has not passed into the BEC, and that the geometric contribution to T_{BKT} is significant.

Section IV contains a comparison of our results both to numerical Monte Carlo calculations and to other approaches. Section V presents our conclusions. Detailed descriptions of the tight-binding model, derivations of our multiorbital pairing fluctuation theory, discussions of the relation between quantum geometry and pair mass, and equations used for the mean field superfluid stiffness and T_{BKT} can be found in the appendices.

II. THEORETICAL FRAMEWORK

A. Band model

Our tight-binding model [26,27] is defined on a square lattice, which splits into two sublattices, $\{A, B\}$, due to a staggered π magnetic flux [40]. The flux is opposite for opposite spins with preserved time reversal symmetry. This symmetry and the absence of spin-orbit coupling reduces the four band pairing problem, including sublattices and spin, to a two-band system with sub-lattices only and we henceforth drop the spin. Here we consider zero center-of-mass momentum and spin singlet pairing.

As a result we have a simple normal state Hamiltonian [26,40] in \mathbf{k} space,

$$H_N(\mathbf{k}) = h_0(\mathbf{k}) + \mathbf{h}(\mathbf{k}) \cdot \mathbf{s} - \mu_F, \quad (1)$$

written in the basis $(c_A^\dagger(\mathbf{k}), c_B^\dagger(\mathbf{k}))$. Here, $\mathbf{s} = (s_x, s_y, s_z)$ are Pauli matrices defined for the sublattice space, $h_0 = -2t_1[\cos 2(k_x + k_y) + \cos 2(k_x - k_y)]$, $h_z = -2t_2[\cos(k_x + k_y) - \cos(k_x - k_y)]$, $h_x + ih_y = -2t[e^{i(-\phi-k_y)} \cos k_y + e^{i(\phi-k_y)} \cos k_x]$, with $\phi = \pi/4$, and μ_F is the fermionic chemical

potential. We set the lattice constant $a_L = 1$. Diagonalizing $H_N(\mathbf{k})$ gives two energy bands, $\xi_\pm(\mathbf{k}) = h_0(\mathbf{k}) \pm |\mathbf{h}(\mathbf{k})| - \mu_F$, with a nonzero Chern number $C = \mp 1$.

For definiteness, following Ref. [26], we consider two sets of hopping parameters: (1) $(t, t_2, t_5) = (1, 1/\sqrt{2}, (1 - \sqrt{2})/4)$ and (2) $(t, t_2, t_5) = (1, 1/\sqrt{2}, 0)$, corresponding, respectively, to a lower bandwidth $W \approx 0.035t$ and $0.83t$, and to a band flatness (ratio) $\mathcal{F} \equiv W/E_g \approx 0.01$ and 0.2 . Both sets have a band gap $E_g = 4t$. Throughout the paper, we consider electron density $n = 0.3$ per square lattice site so that the lower band is only partially filled.

B. Pairing fluctuation theory for $T \geq T_{\text{BKT}}$

Our approach is based on a finite temperature formalism built on the BCS ground state, which can readily be extended to include stronger pairing correlations [33]. It was derived using an equation of motion approach [41,42], following Kadanoff and Martin [43], and extended to address pairing (fluctuations) at an arbitrary strength in the context of BCS-BEC crossover [44]. Compared to other pairing fluctuation theories [45], this formalism is consistent with a BCS-like gap equation and simultaneously a gapless Anderson-Bogoliubov mode in the superfluid phase. This approach has been used to address pairing and pseudogap phenomena in Fermi gases and the cuprates [42,44,46] as well as the effects of spin-orbit coupling on ultracold Fermi gases [28–32], and most recently to address the two dimensional BKT transition [17,47] in several simple cases. In 2D, the natural energy scale parameter, n_B/M_B , enters to describe T_{BKT} .

To determine n_B and M_B we begin with the pair susceptibility $\chi(Q)$. We presume that $\chi(Q)$ assumes a special form (involving one dressed and one bare Green’s function) such that the $Q = 0$ pole of the many body T matrix t_{pg} [44],

$$t_{\text{pg}}(Q) = \frac{-U}{1 - U\chi(Q)}, \quad (2)$$

yields the usual BCS gap equation for the pairing gap Δ_{pg} in the fermionic excitation energy spectrum, $E_\pm(\mathbf{k}) = \sqrt{\xi_\pm(\mathbf{k})^2 + \Delta_{\text{pg}}^2}$. This Δ_{pg} is to be distinguished from the superconducting order parameter Δ_{sc} , which vanishes at any finite T in 2D. Here, $U > 0$ is the strength of a local attractive Hubbard interaction. $Q \equiv (i\Omega_m, \mathbf{q})$ with $\Omega_m = 2m\pi T$ the bosonic Matsubara frequency [40].

Within “the pseudogap approximation” [28,29,32], it is presumed that $t_{\text{pg}}(Q)$ is sharply peaked near $Q = 0$, close to an instability, so that [44]

$$\Delta_{\text{pg}}^2 \equiv -T \sum_{Q \neq 0} t_{\text{pg}}(Q). \quad (3)$$

Following Refs. [17,44,47], for small Q , we Taylor-expand $t_{\text{pg}}^{-1}(Q) = \mathcal{Z}^{-1}(i\Omega_m - \mathbf{q}^2/(2M_B) + \mu_B)$, where

$$\frac{\mu_B}{\mathcal{Z}} = -\frac{1}{U} + \chi(0) = -\frac{1}{U} + \sum_{\mathbf{k} \in \text{RBZ}} \sum_{\alpha=\pm} \frac{\tanh(\beta E_\alpha/2)}{2E_\alpha}. \quad (4)$$

For brevity, we have suppressed the \mathbf{k} dependence on the right-hand side (r.h.s.) “RBZ” stands for reduced Brillouin zone. Here μ_B is the bosonic pair chemical potential. When

μ_B is zero Eq. (4) is recognized as the BCS gap equation, but for the present purposes, we must include nonvanishing μ_B . Note that $t_{pg}(Q)$ can be roughly viewed as a propagator for the preformed pairs with an energy $E_B = \mathbf{q}^2/2M_B - \mu_B$. Both expressions for \mathcal{Z} and $1/M_B$ are obtained as functions of $\{\Delta_{pg}, \mu_F\}$ from the Taylor expansion.

In 2D, with a simple parabolic pair dispersion, Eq. (3) yields [17,47]

$$n_B \equiv \sum_{\mathbf{q}} f_B(E_B) = \mathcal{Z}^{-1} \Delta_{pg}^2 = -\frac{M_B}{2\pi\beta} \ln(1 - e^{\beta\mu_B}), \quad (5)$$

where $\beta = 1/T$, and $f_B(x) = 1/(e^{\beta x} - 1)$. Then we have

$$n_B/M_B = \Delta_{pg}^2/(M_B \mathcal{Z}) = 2 \Delta_{pg}^2 (T_{conv} + T_{geom}), \quad (6)$$

where we have split the contributions to the inverse pair mass into two terms: T_{conv} is the conventional contribution that only depends on the normal state dispersion while T_{geom} is the geometric contribution that carries information about the normal state wave function. Here we present an expression for T_{geom} with details discussed elsewhere [40].

$$T_{geom} = \sum_{\mathbf{k} \in \text{RBZ}} \sum_{(\alpha, \alpha', \eta) = \pm} \frac{1}{4} \left[1 + \eta \frac{\xi_\alpha}{E_\alpha} \right] \times \frac{n_F(\eta E_\alpha) - n_F(-\xi_{\alpha'})}{\eta E_\alpha + \xi_{\alpha'}} (-\alpha\alpha') \frac{1}{4} \sum_{\mu=x,y} \partial_\mu \hat{h} \cdot \partial_\mu \hat{h}, \quad (7)$$

where $n_F(x) = 1/(e^{\beta x} + 1)$ is the Fermi-Dirac distribution, and $\hat{h}(\mathbf{k}) \equiv \mathbf{h}(\mathbf{k})/|\mathbf{h}(\mathbf{k})|$. Interestingly, we see that T_{geom} contains both intra- and interband terms.

Quantum geometry enters into T_{geom} , or equivalently n_B/M_B , through the diagonal components of the quantum metric tensor, $g_{\mu\nu}(\mathbf{k})$:

$$g_{\mu\nu}(\mathbf{k}) = \frac{1}{2} \partial_\mu \hat{h}(\mathbf{k}) \cdot \partial_\nu \hat{h}(\mathbf{k}), \quad (8)$$

where $\{\mu, \nu\} = \{x, y\}$. $g_{\mu\nu}$ is a measure of the distance between two Bloch states in the projective normal state Hilbert space [48]. In the BEC regime, where $n_B = n/2$, $g_{\mu\nu}$ is directly connected to the inverse pair mass $1/M_B$ [40]. We stress that in contrast to other work [34,49] here $1/M_B$ depends on the self consistently determined pairing gap.

Finally, the electrons are subject to the number constraint [17,44,47],

$$n = \sum_{\mathbf{k} \in \text{RBZ}} \sum_{\alpha=\pm} \left[1 - \frac{\xi_\alpha}{E_\alpha} \tanh\left(\frac{\beta E_\alpha}{2}\right) \right]. \quad (9)$$

Equations (4), (5), and (9) form a closed set that can be solved for Δ_{pg} and μ_F , for given (T, n, U) , which also determines the important ratio n_B/M_B .

C. BKT criterion

It was initially proposed in Ref. [50] based on experiments in Fermi gases that the 2D BKT superconducting transition can be reinterpreted as a ‘‘quasicondensation’’ of preformed Cooper pairs. The onset of quasicondensation provides a normal state access to the BKT instability. Here the transition is approached from above, which is complementary to the superfluid phase stiffness based approach (from below). The

quasicondensation onset is quantified through the parameter n_B/M_B which provides a natural 2D energy scale. More specifically, this approach to the BKT transition builds on a Monte-Carlo study of weakly interacting bosons [51] where it was found that at the onset of quasicondensation, i.e., $T = T_{\text{BKT}}$, one has

$$\frac{n_B(T)}{M_B(T)} = \frac{\mathcal{D}_B^{\text{crit}}}{2\pi} T. \quad (10)$$

Here, $\mathcal{D}_B^{\text{crit}}$ is the critical value of the phase space density, $\mathcal{D}_B(T) \equiv n_B \lambda_B^2$ with $\lambda_B = \sqrt{2\pi/M_B T}$ the bosonic thermal de-Broglie wavelength (setting $\hbar = k_B = 1$). This BKT criterion has been supported by experimental studies on atomic Bose gases [52–54].

In general, $\mathcal{D}_B^{\text{crit}}$ depends on the nonuniversal boson-boson interaction strength g_B . In the most general case, g_B is unknown for a fermionic superconductor where Cooper pairs are the emergent composite bosons. However, a small value of g_B appears consistent with the BCS ground state, as the bosonic degrees of freedom enter this wave function in a quasiideal manner. Notably the dependence of $\mathcal{D}_B^{\text{crit}}$ on g_B is logarithmic and therefore weak [51]. Estimates for $\mathcal{D}_B^{\text{crit}}$ for fermionic superfluids range from 4.9 to 6.45 [50,55]. We choose $\mathcal{D}_B^{\text{crit}} = 4.9$ that best fits the data on Fermi gases [55].

D. Isolated flat band limit

It is useful to arrive at some analytical insights on how n_B/M_B depends on the normal state band topology. This can be done in the isolated flat band limit, corresponding to $W \ll U \ll E_g$ (which is in the BEC regime). In this limit, superconductivity is restricted to the lower flat band while the upper band is inactive, and Eq. (6) simplifies to

$$\frac{n_B}{M_B} \approx \Delta_{pg}^2 \sum_{\mathbf{k} \in \text{RBZ}} \frac{\tanh(\beta E_-(\mathbf{k})/2)}{2E_-(\mathbf{k})} \frac{1}{2} \sum_{\mu=x,y} g_{\mu\mu}(\mathbf{k}). \quad (11)$$

Using an inequality between the quantum metric tensor and the normal state band Berry curvature, one obtains [40]

$$\frac{n_B}{M_B} \geq \Delta_{pg}^2 \frac{\tanh(\beta E_-/2)}{4E_-} \frac{|C|}{\pi}, \quad (12)$$

which sets a lower bound for n_B/M_B when $C \neq 0$, i.e., when the system is topologically nontrivial. Here E_- is \mathbf{k} independent and $C = 1$ is the normal state conduction band Chern number. Interestingly, this lower bound is almost identical to the one derived for the MF superfluid phase stiffness in Ref. [22], provided one replaces Δ_{pg} with the MF superconducting order parameter.

III. NUMERICAL RESULTS

In Fig. 1(a), we compare the calculated T_{BKT} from our pairing fluctuation theory with that using the BCS MF superfluid phase stiffness D_s for the case of a flatness parameter $\mathcal{F} = 0.2$. Also plotted is the pairing onset temperature, T^* , well approximated by the mean field transition temperature. In the weak-coupling BCS limit, all three temperatures converge. However, in the strong coupling regime, pairing fluctuations become important and our T_{BKT} is significantly reduced relative to its MF counterpart, as a consequence of an additional

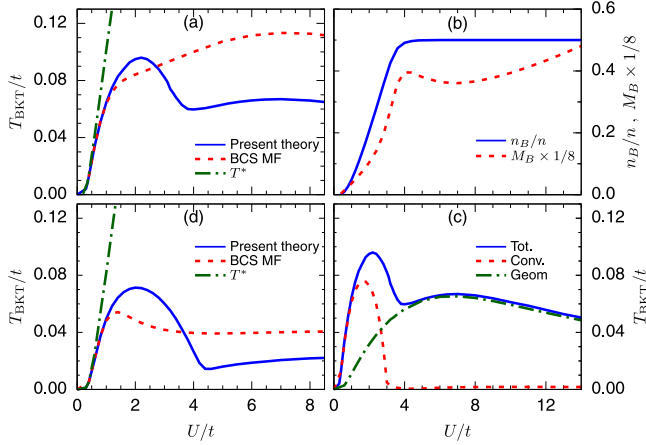


FIG. 1. Behavior of calculated (a) T_{BKT} (labeled “Present theory”) and (b) $\{n_B/n, M_B\}$, (c) decomposition of T_{BKT} (“Tot”) into conventional (“Conv”) and geometric contributions (“Geom”) for topological bands, and (d) T_{BKT} for a nontopological system, as a function of U/t , all with $\mathcal{F} = 0.2$. In comparison, also plotted in (a) and (d) are T^* and T_{BKT} (“BCS MF”) calculated using the MF phase stiffness.

bosonic excitation channel. Unlike the single band theory, where there is a more dramatic T_{BKT} downturn near $U/t \approx 3$, in this multiorbital model the geometric contribution prevents the expected strong decrease [17].

These features can be traced to the behavior of the pair mass, M_B , which is plotted along with n_B in Fig. 1(b). In single band theories with conventional contributions only, due to a large suppression of pair hopping [56] and an increase of pair-pair repulsion with pair density [57], pairs tend to be localized near $U/t \approx 3$, corresponding to $M_B \rightarrow \infty$. The presence of geometric terms prevents this pair mass divergence. Figures 1(a) and 1(b) reveal that, while the small U behavior of T_{BKT} derives from variations in both M_B and n_B , the behavior of T_{BKT} in the BEC regime reflects that of $1/M_B$ only.

To see the importance of the geometric contributions more clearly, in Fig. 1(c), we present a decomposition of T_{BKT} in terms of the conventional and geometric components, by separating the total n_B/M_B into two terms, $(n_B/M_B)^{\text{conv}} \equiv 2\Delta_{\text{pg}}^2 T_{\text{conv}}$ and $(n_B/M_B)^{\text{geom}} \equiv 2\Delta_{\text{pg}}^2 T_{\text{geom}}$. We then apply the BKT criterion in Eq. (10) to each of $\{n_B/M_B, (n_B/M_B)^{\text{conv}}, (n_B/M_B)^{\text{geom}}\}$ to arrive at the three curves in Fig. 1(c). Here we see that T_{BKT} is almost completely geometric at $U/t \gtrsim 3$. The conventional contribution in Fig. 1(c) exhibits a dome-like dependence on U with a maximum at $U \sim W$. Its contribution to T_{BKT} in the pairing fluctuation theory falls precipitously to almost zero at $U/t \approx 3$ and remains extremely small at larger U , resulting from a cancellation between pair hopping and inter-pair repulsion effects [40].

It is instructive to compare with a nontopological superconductor, as shown in Fig. 1(d). Our nontopological bands are constructed by adding a staggered on-site potential to the topologically nontrivial Hamiltonian H_N in Eq. (1) [40]. For a meaningful comparison the trivial band structure is so chosen that both its conduction band width W and band gap E_g

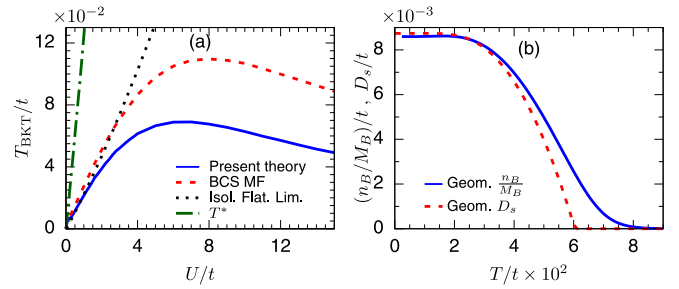


FIG. 2. (a) Characteristic temperatures for the topological $\mathcal{F} = 0.01$ superconductor, and comparison with lower bound of T_{BKT} in the isolated flat band limit (“Isol. Flat. Lim”), obtained using Eqs. (10) and (12). This bound nearly coincides with the calculated T_{BKT} for the range $0.4 \lesssim U/t \lesssim 2$, where the system is in the BEC regime and T_{BKT} is nearly completely geometric. (b) Comparison between the T dependence of n_B/M_B and that of BCS MF D_s at $U/t = 0.5$. For the sake of clarity, only geometric contributions are included.

are comparable to the nontrivial $\mathcal{F} = 0.2$ case. This ensures that the conventional contributions to T_{BKT} , as well as the U dependence of Δ_{pg} and μ_F , are more or less the same in both cases. Comparison of T_{BKT} in Figs. 1(d) and 1(a) at $U/t \gtrsim 4$, where the geometric component dominates, demonstrates that the geometric contribution to T_{BKT} is significantly enhanced in the nontrivial case.

In Fig. 2(a), we present a comparison between the MF and present theory for a nearly flat conduction band, with $\mathcal{F} \approx 0.01$. Just as in Fig. 1(a), pairing fluctuations suppress significantly the transition temperature relative to the mean field result. Also important is the absence of the conventional T_{BKT} peak, seen in Fig. 1(a). There is a small residual feature at $U \sim W = 0.035t$ from the conventional term, which, however, is invisible in the plot. In this nearly flat band limit, T_{BKT} is essentially purely geometric for the entire range of U/t displayed. Notably, even a very small attraction ($U/t \approx 0.3$) puts the system in the BEC regime [40], where n_B/n reaches $1/2$.

Also plotted in Fig. 2(a) are the pairing onset temperature T^* (dot-dashed) along with the lower bound of T_{BKT} in the isolated flat band limit (black dotted line), which is obtained by applying the BKT criterion in Eq. (10) to the r.h.s. of Eq. (12). Interestingly this bound is almost saturated by our calculated T_{BKT} when $0.4 \lesssim U/t \lesssim 2$.

Even with the reduction of T_{BKT} relative to the BCS MF result, in the isolated flat band limit, n_B/M_B is essentially equal to its BCS MF counterpart D_s at $T = T_{\text{BKT}}$ and even for higher temperatures, provided $T \ll T^*$. This can be seen through the comparison in Fig. 2(b) between our n_B/M_B in Eq. (11) and that of the MF D_s , where for clarity we have dropped the small but nonzero conventional term [40].

We turn finally to the physical implications of our calculations for a given 2D superconductor. We quantify the relative size of the geometric terms by use of the dimensionless ratio T^*/T_{BKT} which, importantly, has been shown to be measurable in voltage current (V - I) experiments [39] with consistency checks from STM data. As shown in Fig. 3(a), T^*/T_{BKT} increases monotonically with interaction strength U

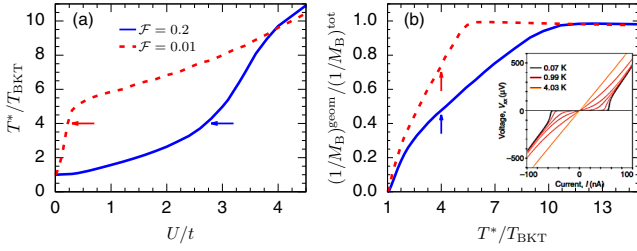


FIG. 3. (a) Calculated T^*/T_{BKT} as a function of U and (b) relative magnitude of the geometric terms plotted as $(n_{\text{B}}/M_{\text{B}})^{\text{geom}}/(n_{\text{B}}/M_{\text{B}})^{\text{tot}}$ as a function of T^*/T_{BKT} , for the topological $\mathcal{F} = 0.2$ and $\mathcal{F} = 0.01$ cases. Arrows correspond to where $T^*/T_{\text{BKT}} = 4$, deduced from the experiments in the inset of (b). (Inset) V - I curves measured at different T for magic-angle TBLG by Cao *et al.* [2]

for both the topological $\mathcal{F} = 0.2$ and $\mathcal{F} = 0.01$ cases, with an even more rapid increase as the system approaches the BEC regime. The fractional contribution of the geometric terms, $(n_{\text{B}}/M_{\text{B}})^{\text{geom}}/(n_{\text{B}}/M_{\text{B}})^{\text{tot}}$, is plotted in Fig. 3(b). Once in the BEC regime, T_{BKT} is dominantly geometric.

To connect to experiments on TBLG, we present the experimental V - I curves for an optimal example [2], in the inset of Fig. 3(b). At $T = T_{\text{BKT}}$ the V - I curve follows a power law, $V \propto R_{\text{N}}I_{\text{c}}(I/I_{\text{c}})^{\alpha}$ with $\alpha = 3$; I_{c} is the critical current and R_{N} is the normal state resistance [58–63]. Importantly, when T reaches T^* the V - I curve fully recovers its normal state Ohmic behavior, $V \propto R_{\text{N}}I$.

From the V - I characteristics by Cao *et al.* [2], we estimate $T^* \approx 4$ K and $T_{\text{BKT}} \approx 1$ K [2], which yield $T^*/T_{\text{BKT}} = 4$. At this ratio, the normalized geometric contribution is about 70% and 50% for $\mathcal{F} = 0.01$ and 0.2, respectively, in Fig. 3(b). Which band flatness ratio is more appropriate for magic angle TBLG depends on one's estimate of the effective bandwidth W and band gap E_{g} . If we take $W \approx 3$ –5 meV, which is the energy range where the bare flat band density of states is appreciable, and $E_{\text{g}} \approx 20$ meV [2], then $\mathcal{F} \approx 0.15$ –0.25. At face value, this suggests that the $\mathcal{F} = 0.2$ case is more relevant to magic angle TBLG. However, one should keep in mind that the estimated W here only provides an upper bound, as the superconductivity in TBLG may be associated with a renormalized and therefore smaller effective band width W . In any case, the geometric contribution to T_{BKT} is significant, ($\gtrsim 50\%$), and the system is in the BCS-BEC crossover regime, although it has not yet passed into the BEC.

A. Further experimental estimates of T^*

We stress that the T^*/T_{BKT} ratio inferred from the V - I characteristics can be quite different from observations in other experiments and with different samples [64–66]. For example, for one superconductor studied in Ref. [65], the ratio is only about 1.4, with $T_{\text{BKT}} = 710$ mK and $T^* \approx 1$ K. This puts the corresponding system in the BCS weak-coupling regime in Fig. 3(a), and consequently the corresponding geometric contribution to T_{BKT} from Fig. 3(b) is only about 10%–20%. However, one should also take note that the T^* read off from all the existing V - I curves is subject to uncertainty since none of the measurements provides a continuous sweep over closely separated temperature intervals.

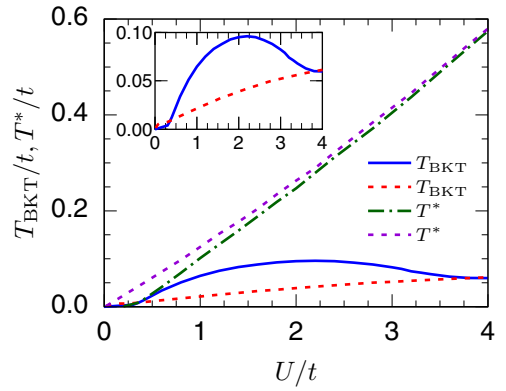


FIG. 4. Results from the pairing fluctuation theory for T_{BKT} and T^* , for both the topological $\mathcal{F} = 0.2$ band (solid blue and dark-green dash-dotted lines) and $\mathcal{F} = 0.01$ bands (red and violet dashed lines). For a better comparison to the Monte-Carlo results [26], only data for U/t up to about 4 are shown. (Inset) Zoomed view of T_{BKT} .

When the V - I measurements are not available, it appears that T^* can be roughly estimated from dc transport. This is based on a temperature feature in the longitudinal resistivity $\rho(T)$, which corresponds to the point where $\rho(T)$ begins to drop below its normal state extrapolation.¹ For example, in transport experiments on a TBLG sample with $T_{\text{BKT}} = 1$ K in Ref. [2], this transport signature yields $T^* = 4 \sim 5$ K, roughly consistent with the value obtained from V - I measurements. While T^* identified in this way is necessarily greater than or equal to T_{BKT} , depending on the carrier density and twist angle, it can be substantially larger. As seen from transport studies in Fig. 1 of Ref. [66], the T^*/T_{BKT} ratio varies from a number close to 1 to a number much larger than 10 as the carrier density is tuned from one side of the superconducting dome to the other in a given sample.²

One can speculate that this wide variation of T^*/T_{BKT} obtained from transport, is unlikely to be due to disorder given that the measurements are on the same sample, though with different carrier density. Instead, variations in Coulomb screening, which crucially depends on the carrier density may play a key role [65–68].

Because of the sensitivity of the effective pairing interaction to band filling and Coulomb screening, determining whether superconducting magic angle TBLG is a weak-coupling or strong-coupling superconductor remains an open question. To firmly settle the issue, further V - I experiments over finely separated temperature intervals in order to establish the temperature for the Ohmic recovery are much needed. As in Ref. [39], for corroboration, these should ultimately be combined with STM measurements of the local pairing gap. STM experiments [67,69–71] on magic angle TBLG to date

¹Similar dc transport signatures of T^* have been observed previously in cuprates [72], although the pseudogap there can have a completely different origin from preformed Cooper pairs.

²Here we ignore the intervening correlated insulating phase at half filling of the lower and upper flat bands and view the two superconducting domes flanking the insulating phase as one.

tend to be limited to the normal state and have not yet reported signatures of the pairing gap or of T^* .

IV. COMPARISON WITH THEORETICAL LITERATURE

Figure 4 makes possible a comparison between our numerical results for T^* and T_{BKT} and the Monte-Carlo (MC) calculations in Ref. [26]. Interestingly, our results are quite similar to the MC results, both qualitatively and even quantitatively. The main difference is a small peak in T_{BKT} at $U/t \approx 2$ for $\mathcal{F} = 0.2$, which derives from the conventional terms and is absent in the MC results. Instead, the MC T_{BKT} for $\mathcal{F} = 0.2$ has a U dependence quite similar to that for $\mathcal{F} = 0.01$, although the magnitude is larger in the former case (see Fig. 1 of Ref. [26]).³ Taken at face value, this suggests that our pairing fluctuation theory overestimates the size of the conventional contribution to T_{BKT} . On the other hand, the MC results may suffer from finite size effects. In any event, this comparison indicates that our pairing fluctuation theory appears to have adequately accounted for the geometric contributions.

Prior to our work, there have been studies of the geometric contribution to the superfluid instability temperature that were associated with beyond mean field Gaussian pairing fluctuations. In a series of papers [34,73], M. Iskin called attention to the geometric contribution in 2D and 3D spin-orbit coupled Fermi gases. Notably, for this specific energy dispersion, the geometric contribution does not play a significant role and the conventional contribution dominates, due to the associated nonflat and unbounded band dispersion. It should be noted that within a Gaussian fluctuation theory, which is most appropriate for 3D superfluids, there does appear an interband geometric contribution [34] similar to our Eq. (7).⁴

Beyond mean field effects and quantum geometry have also been discussed in Ref. [22] in the context of dynamical mean field theory (DMFT). There it was similarly observed that the geometric contribution to the flat band phase stiffness survives, though reduced in magnitude. These DMFT calculations were shown to agree qualitatively with the results of strict mean field theory, not in the BCS regime but in the more strongly correlated BEC limit, where one might expect a mean field approach to be less appropriate. Finally, we note that there are other more analytical approaches which incorporate bosonic fluctuation effects on the superfluid phase stiffness across the entire BCS-BEC crossover [74–76].⁵ While the role of this additional “collective mode” bosonic branch is to degrade the superfluid phase stiffness, as we find here, these schemes have not addressed quantum

geometric effects. Further investigations are needed to resolve these issues.

V. CONCLUSIONS

In summary, we have established the quantum geometric contribution to superfluidity in a pair-fluctuation theory, where these contributions modify the pair mass. In general the geometric contribution dominates in the strong coupling BEC regime and prevents localization of Cooper pairs. We further show how to quantify the magnitude of the geometric contributions in a multiorbital 2D superconductor in terms of the T^*/T_{BKT} ratio. Our analysis was based on important experimental observations [39] which have shown that the two temperature scales (T_{BKT} and T^*) can be extracted from V - I plots. Using estimates of T^*/T_{BKT} from experiments we have presented speculations on magic angle TBLG, concerning the size of the geometric terms and the location of this exotic superconductor within the BCS-BEC crossover.

The rough comparison between theory and experiment in this paper is based on the assumption that the simple model we studied captures some essential features of the band structure of TBLG. While this sets up the general framework and identifies the issues, clearly, a calculation using a realistic band structure is ultimately needed. In our model, the band topology comes from a nonzero spin Chern number. On the other hand, (in the absence of the hBN encapsulating substrate),⁶ the relevant topology for the bare flat bands of TBLG was argued to be different and to correspond to a so called “fragile topology” [9,13,77–79]. Whether this topology is associated with the normal state out of which the superconductivity emerges is still unclear.⁷ However, as demonstrated in a BCS mean field calculation [25], this fragile topology exhibits similar Wannier obstruction effects that can prevent the localization of Cooper pairs and hence enhance 2D superconductivity for a flat band system. Overall, we expect most of our qualitative findings to survive in a more realistic band calculation with fragile topology included. The pairing fluctuation theory that we presented for our two band model can be easily generalized to a more-than-two-band structure, which is more relevant to TBLG. We leave that for future work.

ACKNOWLEDGMENTS

We thank M. Levin for a useful discussion. This work was primarily funded by the University of Chicago Materials Research Science and Engineering Center, and the National Science Foundation under Grant No. DMR-1420709. Q.C. was supported by NSF of China (Grant No. 11774309).

³We note that the results presented in Fig. 1 of Ref. [26] are for electron density $n = 0.5$ per site; while our results are for $n = 0.3$ per site. However, we do not expect the qualitative U dependence of T_{BKT} and T^* to change from $n = 0.5$ to $n = 0.3$.

⁴However, the intraband contribution we identified, the term with $\alpha' = \alpha$ in Eq. (7), was missing.

⁵Unfortunately, these calculations lead to an unusual double valued functional form for the superfluid density.

⁶As shown by recent experimental and theoretical studies [80–83], a coupling of the TBLG to the hBN substrate can break certain symmetry that leads to occurrence of Chern bands and the resulted anomalous Hall effect.

⁷In principle, the normal state bands relevant to the superconductivity can be different from the bare band, due to renormalizations from interactions.

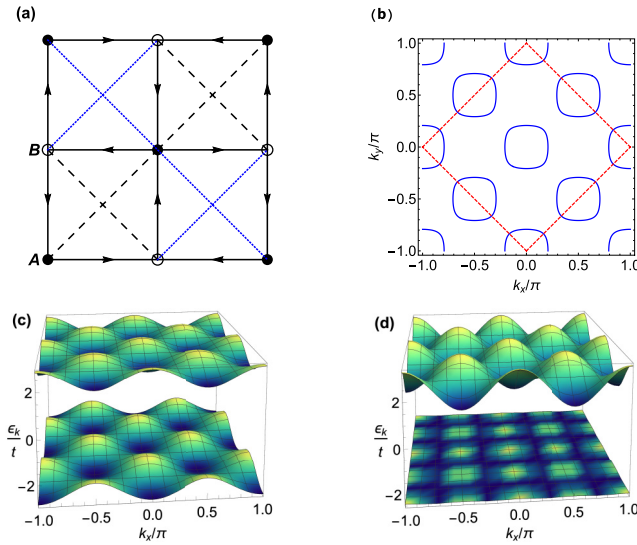


FIG. 5. (a) The tight binding model for H_K . $\{A, B\}$ denote two different sub-lattices, resulting from a staggered π flux. The NN hopping amplitudes are $te^{i\pi/4}$ for spin \uparrow along the direction depicted by the arrows. Black dashed and blue dotted lines show the second NN bond with which the associated hopping amplitudes are t_2 and $-t_2$, respectively. There is also a uniform hopping between the fifth NN sites, which is not shown for clarity. (b) Fermi surfaces (FS), in blue, for the band flatness ratio $\mathcal{F} = 0.2$ at electron density $n = 0.3$ per site. The regime bounded by the red dashed lines defines the reduced Brillouin zone (RBZ). (c) Corresponding band structure for $\mathcal{F} = 0.2$. In the vertical axis, $\epsilon_k = h_0(\mathbf{k}) \pm |\mathbf{h}(\mathbf{k})|$. (d) Band structure for $\mathcal{F} = 0.01$.

APPENDIX A: TIGHT-BINDING MODEL

Our model is defined on a square lattice, with a kinetic energy contribution to the Hamiltonian, H_K , given by

$$H_K = \left\{ \left[-t \sum_{\langle i,j \rangle} e^{i\phi_{ij}^\sigma} c_{i,\sigma}^\dagger c_{j,\sigma} - t_2 \sum_{\langle\langle i,j \rangle\rangle, \sigma} s_{(i,j)2} c_{i,\sigma}^\dagger c_{j,\sigma} - t_5 \sum_{\langle\langle\langle i,j \rangle\rangle\rangle, \sigma} c_{i,\sigma}^\dagger c_{j,\sigma} \right] + h.c. \right\} - \mu_F \sum_i n_i. \quad (\text{A1})$$

Here $c_{i,\sigma}^\dagger$ ($c_{i,\sigma}$) are electron creation (annihilation) operators at site i for spin σ . (t , t_2 , t_5) are the magnitudes of the hopping integrals defined for the nearest neighbor (NN), second NN, and the fifth NN bond on the square lattice, respectively. μ_F is the fermionic chemical potential, and $n_i = \sum_{\sigma=\uparrow,\downarrow} c_{i,\sigma}^\dagger c_{i,\sigma}$ is the electron number at site i . The NN hopping amplitude is modulated by the phase $e^{i\phi_{ij}^\sigma}$, where $\phi_{ij}^\sigma = s_\sigma (\pi/4)$ if the hopping is along the direction of the arrows depicted in Fig. 5. $s_\sigma = +1$ (-1) for spin \uparrow (\downarrow). Because of ϕ_{ij}^σ there is a net $\pm\pi$ flux through each square plaquette for given spin. This flux is staggered from one plaquette to the next (see Fig. 5), which breaks the original lattice translational symmetry and leads to two different sublattices $\{A, B\}$. However, time reversal symmetry is still preserved, because ϕ_{ij}^σ are opposite for opposite spin σ so that the total flux through each plaquette is zero. The sign of the second NN hopping amplitudes, $s_{(i,j)2} = \pm$, is also staggered, as shown in Fig. 5.

Fourier transforming H_K to \mathbf{k} space one finds the following block-diagonal Hamiltonian

$$H_K(\mathbf{k}) = \begin{pmatrix} H_\uparrow(\mathbf{k}) & 0 \\ 0 & H_\downarrow(\mathbf{k}) \end{pmatrix}, \quad (\text{A2})$$

in the basis $(c_{A,\uparrow}^\dagger(\mathbf{k}), c_{B,\uparrow}^\dagger(\mathbf{k}), c_{A,\downarrow}^\dagger(\mathbf{k}), c_{B,\downarrow}^\dagger(\mathbf{k}))$. The diagonal block operating on the same spin is

$$H_\sigma(\mathbf{k}) = h_0(\mathbf{k}) + \mathbf{h}(\mathbf{k}, \phi_\sigma) \cdot \mathbf{s} - \mu_F, \quad (\text{A3})$$

where $\mathbf{s} = (s_x, s_y, s_z)$ are the three Pauli matrices defined for the sublattice space and

$$h_0(\mathbf{k}) = -2t_5 [\cos 2(k_x + k_y) + \cos 2(k_x - k_y)], \quad (\text{A4a})$$

$$h_z(\mathbf{k}) = -2t_2 [\cos(k_x + k_y) - \cos(k_x - k_y)], \quad (\text{A4b})$$

$$h_x(\mathbf{k}, \phi_\sigma) + i h_y(\mathbf{k}, \phi_\sigma) = -2t e^{i(-\phi_\sigma - k_y)} \cos k_y - 2t e^{i(\phi_\sigma - k_y)} \cos k_x. \quad (\text{A4c})$$

$\phi_\sigma = s_\sigma (\pi/4)$. Diagonalizing $H_K(\mathbf{k})$ gives two energy bands, $\xi_\pm(\mathbf{k}) = h_0(\mathbf{k}) \pm |\mathbf{h}(\mathbf{k}, \phi_\sigma)| - \mu_F$, each of which are twofold degenerate due to the spin. The two bands have a nonzero spin dependent Chern number $C_{\alpha\sigma} = -\alpha s_\sigma$, where $\alpha = \pm$.

Although $H_\sigma(\mathbf{k})$ depends on spin due to ϕ_σ , the final result of the time reversal invariant quantity, n_B/M_B which determines the temperature, T_{BKT} , in our theory, is spin independent (see the following Appendix B). Therefore, in the main text, we drop the spin and keep only the spin \uparrow block Hamiltonian, i.e., $H_N \equiv H_\uparrow$ in Eq. (1).

1. Nontopological model Hamiltonian

In Fig. 1(d) of the main text, we also considered a topologically trivial band structure with zero Chern number. The corresponding trivial Hamiltonian is obtained from $H_K(\mathbf{k})$ by adding a staggered on-site potential term

$$H_K^{\text{trivial}}(\mathbf{k}) = H_K(\mathbf{k}) + m_z s_z \otimes \sigma_0, \quad (\text{A5})$$

where σ_0 is the identity matrix in the spin space. The resultant bands from $H_K^{\text{trivial}}(\mathbf{k})$ are trivial if $|m_z| > 4t_2$. Using $(t, t_2, t_5, m_z) = (1, 0.02, 0, -3)$ gives a two-band model with $W \approx 1.2t$ and $E_g \approx 5.8t$, corresponding to $\mathcal{F} = 0.2$. W and E_g are comparable to those of the topological $\mathcal{F} = 0.2$ band.

2. Attractive interaction

For the interaction we choose a local attractive Hubbard model

$$V = -U \sum_i n_{i,\uparrow} n_{i,\downarrow}, \quad (\text{A6})$$

where $U > 0$. We do not discuss the possible origin of this attractive interaction in TBLG, which is not important for our purposes.

APPENDIX B: MULTIORBITAL BCS-BASED PAIRING FLUCTUATION THEORY

In the main text, we have sketched the derivation of our pairing fluctuation theory and outlined the main equations used. In this section, we present the details. We first derive the

expression for our pairing susceptibility and the corresponding many-body T matrix. From the two we then obtain the two central quantities for our calculation of T_{BKT} , n_{B} and M_{B} of the preformed pairs.

1. Pairing susceptibility and many-body T matrix $t_{\text{pg}}(Q)$

Our pairing fluctuation theory is one type of the many BCS-BEC crossover theories. The central assumption behind most of these theories is that even though the original BCS theory is a weak coupling one, the variational BCS ground state wave function has a wider applicability that goes beyond weak coupling [33]. Our theoretical framework is designed such that the $T = 0$ ground state in this theory is identical to the BCS ground state and at the same time it includes pairing fluctuation effects at finite T . Therefore, to derive such a theory for our multiorbital system, we first consider the corresponding BCS mean field problem.

Within the BCS mean field, the Cooper pairing instability can be derived from the pairing vertex function $\Gamma(Q)$. Assuming a local s -wave singlet pairing order parameter $\hat{\Delta}_{\text{sc}}(\mathbf{k}) = \Delta_{\text{sc}} i\sigma_y$, one can show that [29]

$$\frac{1}{\Gamma(Q)} = -\frac{1}{U} + \chi_0(Q), \quad (\text{B1})$$

$$\chi_0(Q) = \frac{T}{2} \sum_K \text{Tr}[\mathcal{G}_0(K) i\sigma_y \tilde{\mathcal{G}}_0(K-Q) (-i\sigma_y)]. \quad (\text{B2})$$

$\chi_0(Q)$ is the bare pairing susceptibility. $K = (\omega_n, \mathbf{k})$ with $\omega_n = (2n+1)\pi T$ is the fermionic Matsubara frequency. The summation over \mathbf{k} should be restricted to the reduced Brillouin zone due to the unit cell doubling in real space. The trace is with respect to both sublattice and spin. $\mathcal{G}_0(K)$ and $\tilde{\mathcal{G}}_0(K)$ are the normal state electronic and hole Green's function matrices, whose definitions are

$$\mathcal{G}_0(K) = 1/(i\omega_n - H_K(\mathbf{k})), \quad (\text{B3})$$

$$\tilde{\mathcal{G}}_0(K) \equiv -[\mathcal{G}_0(-K)]^T. \quad (\text{B4})$$

$1/\Gamma(Q=0) = 0$ defines the BCS mean field $T_{c, \text{BCS}}$, which will be taken as an estimate for the pairing onset temperature T^* in our theory, i.e., $T^* = T_{c, \text{BCS}}$.

Correspondingly, the mean field BCS gap equation for Δ_{sc} is given by

$$-\frac{1}{U} + \frac{T}{2} \sum_K \text{Tr}[\mathcal{G}(K) i\sigma_y \tilde{\mathcal{G}}_0(K) (-i\sigma_y)] = 0, \quad (\text{B5})$$

where $\mathcal{G}(K)$ is the electron Green's function with the superconducting pairing self-energy $\Sigma_{\text{sc}}(K)$ included

$$[\mathcal{G}(K)]^{-1} = [\mathcal{G}_0(K)]^{-1} - \Sigma_{\text{sc}}(K), \quad (\text{B6})$$

$$\Sigma_{\text{sc}}(K) = \Delta_{\text{sc}}^2 \tilde{\mathcal{G}}_0(K). \quad (\text{B7})$$

The zero temperature solution of Δ_{sc} to the above gap equation gives the BCS ground state.

Now we construct the pairing fluctuation theory. To account for the effects of scattering from noncondensed pairs on fermions, we include another pairing self-energy, Σ_{pg} , into the dressed electronic Green's function \mathcal{G}

$$[\mathcal{G}(K)]^{-1} = [\mathcal{G}_0(K)]^{-1} - \Sigma_{\text{pg}}(K). \quad (\text{B8})$$

Σ_{pg} results from scatterings of electrons from noncondensed pairs, to be distinguished from Σ_{sc} which represents a true condensate. In three dimension (3D) we should include Σ_{sc} as in the BCS mean field theory. In 2D and at finite temperature, which is what we focus on, $\Sigma_{\text{sc}} \equiv 0$ since there is no true long range superconducting order parameter.

$\Sigma_{\text{pg}}(K)$ is related to the many-body T matrix $t_{\text{pg}}(Q)$ by

$$\Sigma_{\text{pg}}(K) = -T \sum_{Q \neq 0} t_{\text{pg}}(Q) \tilde{\mathcal{G}}_0(K-Q). \quad (\text{B9})$$

All pair scattering effects are encapsulated in $t_{\text{pg}}(Q)$. Under the T -matrix approximation that has been widely used to understand BCS-BEC crossovers [44,56]

$$\frac{1}{t_{\text{pg}}(Q)} = -\frac{1}{U} + \chi(Q), \quad (\text{B10})$$

where

$$\chi(Q) = \frac{T}{2} \sum_K \text{Tr}[\mathcal{G}(K) i\sigma_y \tilde{\mathcal{G}}_0(K-Q) (-i\sigma_y)]. \quad (\text{B11})$$

In the course of the developments of BCS-BEC crossover theories, there was a debate on whether the two Green's functions used in the expression of $\chi(Q)$ should be $\mathcal{G}_0 \tilde{\mathcal{G}}_0$, or $\mathcal{G} \tilde{\mathcal{G}}$, or $\mathcal{G} \tilde{\mathcal{G}}_0$. We choose the asymmetric form, $\mathcal{G} \tilde{\mathcal{G}}_0$, so that in 3D, when the superconducting transition is interpreted as a BEC of Cooper pairs, the ground state of this pairing fluctuation theory is given by the BCS wave function [44]. This is reflected in the pole structure of the T matrix, determined by $1/t_{\text{pg}}(0) = 0$ which yields the usual BCS gap equation for Δ_{pg} . It should be noted that the asymmetric form $\mathcal{G} \tilde{\mathcal{G}}_0$ can in fact be derived within the equation of motion approach [43,84].

To proceed further, we note that for small pair chemical potential we may approximate $t_{\text{pg}}(Q)$, noting that it is sharply peaked near $Q = 0$ so that Eq. (B9) can be written as

$$\Sigma_{\text{pg}}(K) \approx \Delta_{\text{pg}}^2 \tilde{\mathcal{G}}_0(K), \quad (\text{B12})$$

$$\Delta_{\text{pg}}^2 \equiv -T \sum_{Q \neq 0} t_{\text{pg}}(Q). \quad (\text{B13})$$

We refer to this as the ‘‘pg approximation,’’ which (near the superconducting instability) is supported by numerical evidence [42]. Equation (B12) is an analog to the BCS pairing self-energy given in Eq. (B7). Just as in the BCS mean field theory, the above form of $\Sigma_{\text{pg}}(K)$ leads to a pseudogap Δ_{pg} in the fermionic excitation energy spectrum $E_{\pm}(\mathbf{k}) = \sqrt{\xi_{\pm}(\mathbf{k})^2 + \Delta_{\text{pg}}^2}$, which reflects the binding strength of noncondensed Cooper pairs.

For the Hamiltonian that is block diagonal in Eq. (A2), we can carry out the spin trace in Eq. (B11) and write

$$\chi(Q) = \frac{1}{2} [\chi_{\uparrow\downarrow}(Q) + \chi_{\downarrow\uparrow}(Q)], \quad (\text{B14})$$

where

$$\chi_{\sigma\bar{\sigma}}(Q) = T \sum_K \text{Tr}[\mathcal{G}_{\sigma}(K) \tilde{\mathcal{G}}_{0,\bar{\sigma}}(K-Q)]. \quad (\text{B15})$$

$\bar{\sigma} = \uparrow (\downarrow)$ if $\sigma = \downarrow (\uparrow)$. \mathcal{G}_{σ} and $\tilde{\mathcal{G}}_{0,\bar{\sigma}}$ are the spin σ block of \mathcal{G} and the spin $\bar{\sigma}$ block of $\tilde{\mathcal{G}}_0$, respectively. Substituting the definitions of $\mathcal{G}_{\sigma}(K)$ and $\mathcal{G}_{0,\bar{\sigma}}(K)$ into the expression for

$\chi_{\sigma\bar{\sigma}}(Q)$ and completing the fermionic Matsubara sum, one gets

$$\begin{aligned} \chi_{\sigma\bar{\sigma}}(Q) &= \sum_{\mathbf{k} \in \text{RBZ}} \sum_{\{\alpha, \alpha', \eta\} = \pm} \frac{1}{2} \left[1 + \eta \frac{\xi_{\alpha}(\mathbf{k})}{E_{\alpha}(\mathbf{k})} \right] \\ &\times \frac{n_F(\eta E_{\alpha}(\mathbf{k})) - n_F(-\xi_{\alpha'}(\mathbf{k} - \mathbf{q}))}{i\Omega_m - \eta E_{\alpha}(\mathbf{k}) - \xi_{\alpha'}(\mathbf{k} - \mathbf{q})} \\ &\times \text{Tr}[\hat{P}_{\alpha, \sigma}(\mathbf{k}) \hat{P}_{\alpha', \sigma}(\mathbf{k} - \mathbf{q})], \end{aligned} \quad (\text{B16})$$

where $n_F(x) = 1/(e^{\beta x} + 1)$ with $\beta = 1/T$ is the Fermi-Dirac distribution function and $\text{Tr}[\dots]$ is with respect to the sublattice subspace.

$$\hat{P}_{\alpha, \sigma}(\mathbf{k}) \equiv \frac{1}{2} [1 + \alpha \hat{\mathbf{h}}(\mathbf{k}, \phi_{\sigma}) \cdot \mathbf{s}] \quad (\text{B17})$$

is the projection operator defined for the normal state band with energy $\xi_{\alpha}(\mathbf{k})$ and spin σ . $\hat{\mathbf{h}}(\mathbf{k}, \phi_{\sigma}) \equiv \mathbf{h}(\mathbf{k}, \phi_{\sigma})/|\mathbf{h}(\mathbf{k}, \phi_{\sigma})|$. Carrying out the trace in Eq. (B16) leads to

$$\text{Tr}[\hat{P}_{\alpha, \sigma}(\mathbf{k}) \hat{P}_{\alpha', \sigma}(\mathbf{k} - \mathbf{q})] = \frac{1 + \alpha\alpha' \hat{\mathbf{h}}(\mathbf{k}, \phi_{\sigma}) \cdot \hat{\mathbf{h}}(\mathbf{k} - \mathbf{q}, \phi_{\sigma})}{2}. \quad (\text{B18})$$

$$T_{\text{conv}} = \sum_{\mathbf{k} \in \text{RBZ}} \sum_{\{\alpha, \eta\} = \pm} \frac{\eta}{4E_{\alpha}} \left\{ (\partial_x \xi_{\alpha})^2 2 \left[\frac{n_F(\eta E_{\alpha}) - n_F(-\xi_{\alpha})}{(\eta E_{\alpha} + \xi_{\alpha})^2} + \frac{\beta n_F(\xi_{\alpha}) n_F(-\xi_{\alpha})}{\eta E_{\alpha} + \xi_{\alpha}} \right] - \partial_x^2 \xi_{\alpha} \frac{n_F(\eta E_{\alpha}) - n_F(-\xi_{\alpha})}{\eta E_{\alpha} + \xi_{\alpha}} \right\}, \quad (\text{B21a})$$

$$T_{\text{geom}} = \sum_{\mathbf{k} \in \text{RBZ}} \sum_{\{\alpha, \alpha', \eta\} = \pm} \frac{1}{4} \left[1 + \eta \frac{\xi_{\alpha}}{E_{\alpha}} \right] \frac{n_F(\eta E_{\alpha}) - n_F(-\xi_{\alpha'})}{\eta E_{\alpha} + \xi_{\alpha'}} (-\alpha\alpha') \frac{1}{2} \partial_x \hat{\mathbf{h}} \cdot \partial_x \hat{\mathbf{h}}, \quad (\text{B21b})$$

where $\partial_x \equiv \partial_{k_x}$, and, for brevity, we have suppressed the \mathbf{k} dependence. The conventional term, T_{conv} , is derived from the q_x derivative of the factors other than $\text{Tr}[\dots]$ in Eq. (B16); while the geometric term, T_{geom} , comes solely from that of the trace factor,

$$\partial_{q_x}^2 \text{Tr}[\hat{P}_{\alpha, \sigma}(\mathbf{k}) \hat{P}_{\alpha', \sigma}(\mathbf{k} - \mathbf{q})]_{\mathbf{q}=0} = (-\alpha\alpha') \frac{1}{2} \partial_{k_x} \hat{\mathbf{h}}(\mathbf{k}, \phi_{\sigma}) \cdot \partial_{k_x} \hat{\mathbf{h}}(\mathbf{k}, \phi_{\sigma}). \quad (\text{B22})$$

T_{geom} depends on not only the normal state energy dispersion but also its wave functions, through the projection operators in the trace factor. This is in sharp contrast to T_{conv} . The scalar product, $\frac{1}{2} \partial_x \hat{\mathbf{h}} \cdot \partial_x \hat{\mathbf{h}}$, can be identified with the xx component of the quantum metric tensor which will be defined and discussed in detail in Appendix C.

We note that although $\hat{\mathbf{h}}(\mathbf{k}, \phi_{\sigma})$ depends on spin due to ϕ_{σ} , $\frac{1}{2} \partial_x \hat{\mathbf{h}} \cdot \partial_x \hat{\mathbf{h}}$ does not because it is even in the sign of ϕ_{σ} . As a result, $\{\chi(0), b, c\}$ are all spin independent. So are the characteristic parameters for the noncondensed bosons such as n_B and M_B .

3. n_B and M_B

Next we calculate n_B and M_B from $\{\chi(0), b, c\}$. Substituting Eq. (B19) into Eq. (B10) leads to

$$t_{\text{pg}}(Q) \approx \frac{\mathcal{Z}}{i\Omega_m - \mathbf{q}^2/(2M_B) + \mu_B}, \quad (\text{B23})$$

with

$$\mathcal{Z} = 1/b, \quad (\text{B24a})$$

$$\mu_B = \frac{-1/U + \chi(0)}{b}, \quad (\text{B24b})$$

$$M_B = b/(2c). \quad (\text{B24c})$$

The quantity $t_{\text{pg}}(Q)$ in Eq. (B23) can be interpreted as the propagator for noncondensed pairs with an energy dispersion $E_B = \mathbf{q}^2/2M_B - \mu_B$, with M_B the effective pair mass and μ_B the corresponding bosonic chemical potential. Then from Eqs. (B13) and (B23) one can relate the areal density of

2. Small Q expansion of $\chi(Q)$

Within the ‘‘pg approximation,’’ one can make the the following small Q expansion for $\chi(Q)$ [17,44,47],

$$\chi(Q) \approx \chi(0) + b i \Omega_m - c \mathbf{q}^2, \quad (\text{B19})$$

where $\Omega_m = 2m\pi T$ is the bosonic Matsubara frequency, and

$$\chi(0) = \sum_{\mathbf{k} \in \text{RBZ}} \sum_{\alpha = \pm} \frac{1 - 2n_F(E_{\alpha})}{2E_{\alpha}}, \quad (\text{B20a})$$

$$b = - \sum_{\mathbf{k} \in \text{RBZ}} \sum_{\{\alpha, \eta\} = \pm} \frac{\eta}{2E_{\alpha}} \frac{n_F(\eta E_{\alpha}) - n_F(-\xi_{\alpha})}{\eta E_{\alpha} + \xi_{\alpha}}, \quad (\text{B20b})$$

$$c = - \frac{1}{2} \frac{\partial^2}{\partial q_x^2} \chi(Q) \Big|_{Q=0} \equiv T_{\text{conv}} + T_{\text{geom}}. \quad (\text{B20c})$$

Here to determine the coefficient c , we use only the q_x^2 component of the $\chi(Q)$ expansion, since the system possesses a C_4 rotational symmetry.

For our later discussion on quantum geometry we have broken up c into two separate terms,

noncondensed pairs, n_B , to Δ_{pg}^2 by

$$n_B \equiv \sum_{\mathbf{q}} f_B(E_B) = \frac{\Delta_{\text{pg}}^2}{\mathcal{Z}} = \frac{M_B}{2\pi\beta} \{-\ln[1 - e^{\beta\mu_B}]\}, \quad (\text{B25})$$

where $f_B(x) = 1/(e^{\beta x} - 1)$ is the Bose-Einstein distribution. To obtain the r.h.s. of the last equality we have neglected the upper bound in the \mathbf{q} summation which is associated with a lattice. This is consistent with the pg approximation which implies, near the instability, a fast decrease of $t_{\text{pg}}(Q)$ at large Q .

Equations (B24) and (B25) combined together yield one independent nonlinear equation for two unknowns, Δ_{pg} and μ_B , in terms of $\{T, n, U\}$. The other independent equation comes from the electron density constraint [17,44,47]

$$n = \sum_{\mathbf{k} \in \text{RBZ}} \sum_{\alpha = \pm} \left[1 - \frac{\xi_{\alpha}(\mathbf{k})}{E_{\alpha}(\mathbf{k})} \tanh \frac{\beta E_{\alpha}(\mathbf{k})}{2} \right]. \quad (\text{B26})$$

Solving the combined Eqs. (B24) to (B26) for given $\{T, n, U\}$ numerically we are able to compute Δ_{pg} and μ_{F} , from which n_{B} and M_{B} can be determined. We then apply the BKT criterion, $n_{\text{B}}(T)/M_{\text{B}}(T) = (\mathcal{D}_{\text{B}}^{\text{crit}}/2\pi)T$, to determine T_{BKT} .

Using Eq. (B26) one can also rewrite the bosonic density as [28]

$$n_{\text{B}} = \frac{n}{2} - \sum_{\mathbf{k} \in \text{RBZ}} \sum_{\alpha=\pm} n_{\text{F}}(\xi_{\alpha}(\mathbf{k})). \quad (\text{B27})$$

This equation shows that n_{B} increases with U for given temperature since μ_{F} decreases with U . As U increases, the zero temperature μ_{F} becomes negative, i.e., lower than the conduction band bottom, at a certain value of U . Beyond this value n_{B} saturates to $n/2$ at $T = 0$ since $n_{\text{F}}(\xi_{\alpha}(\mathbf{k})) = 0$ for all \mathbf{k} . The saturation defines the entrance to the BEC regime. However, we notice that at finite T , the point where μ_{F} becomes negative and the saturation onset of n_{B} do not occur concomitantly at the same U as $n_{\text{F}}(\xi_{\alpha}(\mathbf{k})) \neq 0$ even if μ_{F} is negative.

To see clearly where the quantum metric enters the bosonic parameters, we combine n_{B} and M_{B} and write the ratio as

$$n_{\text{B}}/M_{\text{B}} = 2 \Delta_{\text{pg}}^2 c = 2 \Delta_{\text{pg}}^2 (T_{\text{conv}} + T_{\text{geom}}), \quad (\text{B28})$$

where Eqs. (B25), (B24), and (B20c) have been used. This equation shows explicitly that the quantum metric affects T_{BKT} through the ratio $n_{\text{B}}/M_{\text{B}}$, or $1/M_{\text{B}}$ in the BEC regime, where $n_{\text{B}} = n/2 = \text{const}$.

4. Large U limit of $n_{\text{B}}/M_{\text{B}}$ at $T = T_{\text{BKT}}$

In the $U \gg E_{\text{g}}$ limit, $T_{\text{conv}} \ll T_{\text{geom}}$ so that one can neglect T_{conv} in Eq. (B28). Also in this case, μ_{F} is large negative and T_{BKT} is much smaller than $|\xi_{\alpha}|$ and E_{α} so that one can take $T \approx 0$ in evaluating T_{geom} in Eq. (B21b). All Fermi functions $n_{\text{F}}(x)$ become either 0 or 1, so that one can simplify T_{geom} and rewrite Eq. (B28) as

$$\frac{n_{\text{B}}}{M_{\text{B}}} \approx \left(\sum_{\mathbf{k}} \frac{1}{2} \partial_x \hat{h} \cdot \partial_x \hat{h} \right) \frac{2|\mu_{\text{F}}| + |\mu_{\text{F}}|^2/E_0 - E_0}{2E_0^2(E_0 + |\mu_{\text{F}}|)^2} \Delta_{\text{pg}}^2 E_{\text{g}}^2, \quad (\text{B29})$$

where $E_0 \equiv \sqrt{\mu_{\text{F}}^2 + \Delta_{\text{pg}}^2}$. Because both Δ_{pg} and $|\mu_{\text{F}}|$ are proportional to U at $U \gg E_{\text{g}}$, we conclude that in the large U limit $n_{\text{B}}/M_{\text{B}} \propto E_{\text{g}}^2/U$.

APPENDIX C: QUANTUM GEOMETRY AND THE PAIR MASS

Equation (B28) suggests that the quantum metric can play an important role in determining T_{BKT} through the T_{geom} term in $n_{\text{B}}/M_{\text{B}}$, if the conventional contribution is small. In this section we introduce the definition for the quantum metric, discuss the physical picture behind its interplay with delocalization of noncondensed pairs, and elucidate the role of the normal state band topology in such an interplay. The latter becomes most clear in the isolated flat band limit, where we show $n_{\text{B}}/M_{\text{B}}$ is lower bounded by the nontrivial band topology.

The quantum metric tensor, $g_{\mu\nu}^{\alpha\sigma}(\mathbf{k})$ with $\{\mu, \nu\} = \{x, y\}$, is defined for each $\alpha\sigma$ normal state band. It represents a distance in the projective Hilbert space between two states

$\psi_{\alpha\sigma}(\mathbf{k})$ and $\psi_{\alpha\sigma}(\mathbf{k} + d\mathbf{k})$: $ds^2 \equiv 1 - |(\psi_{\alpha\sigma}(\mathbf{k})|\psi_{\alpha\sigma}(\mathbf{k} + d\mathbf{k}))|^2 = \frac{1}{2} g_{\mu\nu}^{\alpha\sigma}(\mathbf{k}) dk_{\mu} dk_{\nu} + \mathcal{O}((dk)^3)$ [48,85]. Here $\psi_{\alpha\sigma}(\mathbf{k})$ is an eigenstate of $H_{\mathbf{K}}(\mathbf{k})$ in Eq. (A2) with the quantum number $\alpha = \pm$ and $\sigma = \{\uparrow, \downarrow\}$. Note that $g_{\mu\nu}^{\alpha\sigma}(\mathbf{k})$ is independent of the arbitrary $U(1)$ phase of $\psi_{\alpha\sigma}(\mathbf{k})$, and is therefore gauge invariant. By definition it is also positive definite.

The quantum metric tensor can be combined with the Berry curvature, $\mathcal{F}_{\mu\nu}^{\alpha\sigma}$, to define a quantum geometric tensor $\mathcal{R}_{\mu\nu}^{\alpha\sigma}$ [48]:

$$\mathcal{R}_{\mu\nu}^{\alpha\sigma} \equiv 2 \text{Tr}[\hat{P}_{\alpha,\sigma} \partial_{k_{\mu}} \hat{P}_{\alpha,\sigma} \partial_{k_{\nu}} \hat{P}_{\alpha,\sigma}] = g_{\mu\nu}^{\alpha\sigma} + i\mathcal{F}_{\mu\nu}^{\alpha\sigma}/2. \quad (\text{C1a})$$

Both $g_{\mu\nu}^{\alpha\sigma}$ and $\mathcal{F}_{\mu\nu}^{\alpha\sigma}$ are real. Using the definition of $\hat{P}_{\alpha,\sigma}$ in Eq. (B17), one obtains

$$g_{\mu\nu}^{\alpha\sigma}(\mathbf{k}) = \frac{1}{2} \partial_{\mu} \hat{h}(\mathbf{k}, \phi_{\sigma}) \cdot \partial_{\nu} \hat{h}(\mathbf{k}, \phi_{\sigma}), \quad (\text{C2a})$$

$$\mathcal{F}_{\mu\nu}^{\alpha\sigma}(\mathbf{k}) = \alpha \epsilon_{\mu\nu} \hat{h}(\mathbf{k}, \phi_{\sigma}) \cdot [\partial_{\mu} \hat{h}(\mathbf{k}, \phi_{\sigma}) \times \partial_{\nu} \hat{h}(\mathbf{k}, \phi_{\sigma})], \quad (\text{C2b})$$

where $\epsilon_{\mu\nu} = -\epsilon_{\nu\mu}$ is the Levi-Civita symbol. $g_{\mu\nu}^{\alpha\sigma}$ is even under time reversal, and therefore independent of the spin σ . In contrast, $\mathcal{F}_{\mu\nu}^{\alpha\sigma}$ is odd under time reversal, and therefore opposite for opposite spin. As a result, $g_{\mu\nu}^{\alpha\sigma}$ in Eq. (C2a) is independent of $\{\alpha\sigma\}$ for our model.

From its definition one can prove that $\mathcal{R}_{\mu\nu}^{\alpha\sigma}$ is positive definite [21,25], resulting an inequality between $g_{\mu\nu}^{\alpha\sigma}$ and $\mathcal{F}_{\mu\nu}^{\alpha\sigma}$: $g_{xx}^{\alpha\sigma} g_{yy}^{\alpha\sigma} \geq (\mathcal{F}_{xy}^{\alpha\sigma})^2/4$. The inequality implies

$$\text{Tr}[g_{\mu\nu}^{\alpha\sigma}] \geq 2\sqrt{g_{xx}^{\alpha\sigma} g_{yy}^{\alpha\sigma}} \geq |\mathcal{F}_{xy}^{\alpha\sigma}|. \quad (\text{C3})$$

Here Tr is with respect to $\{\mu\nu\}$. Equation (C3) shows that in general a nonzero Chern number, which necessarily implies a nonzero $|\mathcal{F}_{xy}^{\alpha\sigma}|$, enhances the magnitude of the quantum metric tensor. The physics behind this can be understood in terms of the ‘‘Wannier obstruction.’’ Normal state Wannier functions $|\psi_{\alpha\sigma}(\mathbf{R})\rangle$ can be constructed from the Bloch wave function $|\psi_{\alpha\sigma}(\mathbf{k})\rangle$. $|\psi_{\alpha\sigma}(\mathbf{R})\rangle$ is in general not gauge invariant because of the $U(1)$ phase ambiguity in defining $|\psi_{\alpha\sigma}(\mathbf{k})\rangle$. Consequently, the spatial spread of $|\psi_{\alpha\sigma}(\mathbf{R})\rangle$ contains both a gauge invariant and noninvariant part [37,38]. Interestingly, the former is equal to $\sum_{\mathbf{k}} \text{Tr}[g_{\mu\nu}^{\alpha\sigma}]$. If the $\alpha\sigma$ band is topologically trivial, then an exponentially localized $|\psi_{\alpha\sigma}(\mathbf{R})\rangle$ can be constructed by choosing a proper gauge. On the other hand, if the $\alpha\sigma$ band is nontrivial, then this is impossible. This is known as the ‘‘Wannier obstruction’’ [37,38], which implies a larger Wannier function spread, and therefore a larger $\sum_{\mathbf{k}} \text{Tr}[g_{\mu\nu}^{\alpha\sigma}]$.

The enhancement of $\text{Tr}[g_{\mu\nu}^{\alpha\sigma}]$ due to nontrivial band topology also affects the pairing state through $n_{\text{B}}/M_{\text{B}}$. The latter reflects the degree of delocalization of the noncondensed pairs. Both a larger n_{B} and smaller M_{B} imply a larger overlap between individual pair wave functions, and therefore more delocalized pairs. How delocalized the pairs are must be connected to how delocalized the normal state Wannier orbitals are. Therefore it is not surprising that $g_{\mu\nu}^{\alpha\sigma}$, which provides a measure of how delocalized the normal states are, enters the expression of $n_{\text{B}}/M_{\text{B}}$ through T_{geom} in Eq. (B21b). However, $g_{\mu\nu}^{\alpha\sigma}$ appears in a complicated way because both the two normal bands can contribute, and because both intra- and interband processes matter. Interestingly, the inter- and

intraband contributions in Eq. (B21b) carry opposite signs; the former partially cancels the latter which is positive.

The above qualitative discussion suggests that in general, a nontrivial band topology enhances the quantum metric, which in turn increases n_B/M_B . This emerges most clearly in the isolated flat band limit, which was also heavily discussed in the literature addressing the superfluid phase stiffness D_s [21,22,24,25], where a lower bound for the mean field D_s was found. In the following, we show that a similar bound exists for n_B/M_B in this limit.

1. Isolated flat band limit

The isolated flat band limit for the Hamiltonian in Appendix B is defined at U such that $W \ll U \ll E_g$. This regime corresponds to a BEC superconductor. In this limit, superconductivity mainly occurs in the lower flat energy band while the upper one is inactive. As a consequence, all terms involving the upper energy band in the equations for $\{T_{\text{conv}}, T_{\text{geom}}\}$ drop out. Also, the lower flat band term in T_{conv} can be neglected because the band is flat. The only remaining term comes from T_{geom} , which involves the lower flat band. Then from Eq. (B28), one finds

$$\frac{n_B}{M_B} = \Delta_{\text{pg}}^2 \sum_{\mathbf{k} \in \text{RBZ}} \frac{\tanh(\beta E_-(\mathbf{k})/2)}{2E_-(\mathbf{k})} g_{xx}(\mathbf{k}), \quad (\text{C4})$$

where we have left the band dependence of $g_{\mu\nu}^{\alpha\sigma}$ unspecified since it is the same for different bands.

Interestingly, this expression for n_B/M_B is almost identical to that of the BCS mean field D_s in the same limit (see Eq. (D6) of Appendix D and also Ref. [22]). The only difference is that the gap parameter in n_B/M_B is the pseudogap Δ_{pg} while that in D_s is the BCS mean field superconducting order parameter.

Using Eq. (C3) and $g_{xx} = g_{yy}$, one can derive the following lower bound for n_B/M_B

$$\begin{aligned} \frac{n_B}{M_B} &\geq \Delta_{\text{pg}}^2 \frac{\tanh(\beta E_-/2)}{4E_-} \sum_{\mathbf{k} \in \text{RBZ}} |\mathcal{F}_{xy}(\mathbf{k})| \\ &\geq \Delta_{\text{pg}}^2 \frac{\tanh(\beta E_-/2)}{4E_-} \left| \sum_{\mathbf{k} \in \text{RBZ}} \mathcal{F}_{xy}(\mathbf{k}) \right| \\ &= \Delta_{\text{pg}}^2 \frac{\tanh(\beta E_-/2)}{4E_-} \frac{|C|}{\pi}. \end{aligned} \quad (\text{C5})$$

E_- is \mathbf{k} independent since the band is flat. We dropped the band dependence of the Berry curvature $\mathcal{F}_{xy}^{\alpha\sigma}(\mathbf{k})$ and also that of the Chern number $C_{\alpha\sigma}$, since their absolute values are the same for all bands. To obtain the last line we have used Eq. (C2b). This line clearly shows that n_B/M_B is bounded below when the flat band has a nonzero Chern number, i.e., it is topologically nontrivial.

APPENDIX D: MEAN FIELD CALCULATION OF $D_s(T)$ and T_{BKT}

In Figs. 1 and 2 of the main text, we have included the mean field results of D_s and T_{BKT} for comparison. This section gives a summary of the main equations used.

We start with the BCS mean field gap equation

$$\frac{1}{U} = \sum_{\mathbf{k} \in \text{RBZ}} \sum_{\alpha=\pm} \frac{1}{2E_\alpha(\mathbf{k})} \tanh\left(\frac{\beta E_\alpha(\mathbf{k})}{2}\right), \quad (\text{D1})$$

where $E_\alpha \equiv \sqrt{\xi_\alpha^2 + \Delta_{\text{sc}}^2}$ with Δ_{sc} the BCS mean field superconducting gap. This equation is derived from Eq. (B5). The electron density equation is the same as in Eq. (B26). Solving the two equations for given T and U , one obtains Δ_{sc} and μ_F .

From the mean field Δ_{sc} and μ_F , we calculate the mean field D_s by (for derivations see Refs. [22,24])

$$D_s = \frac{1}{4} \sum_{\mathbf{k} \in \text{RBZ}} \sum_{\{i,j\}=\{1,2,3,4\}} \frac{n_F(\mathcal{E}_j) - n_F(\mathcal{E}_i)}{\mathcal{E}_i - \mathcal{E}_j} \{ \langle \Psi_i | \partial_x H_{\text{BdG}}[\Delta_{\text{sc}} = 0] | \Psi_j \rangle \langle \Psi_j | \partial_x H_{\text{BdG}} | \Psi_i \rangle - \langle \Psi_i | j_x^\dagger | \Psi_j \rangle \langle \Psi_j | j_x | \Psi_i \rangle \}, \quad (\text{D2})$$

where $\mathcal{E}_i = \pm E_\pm$ and $|\Psi_i\rangle$ are eigenenergies and eigenvectors of the following 4×4 mean field BdG Hamiltonian matrix

$$H_{\text{BdG}}(\mathbf{k}) = \begin{pmatrix} H_\uparrow(\mathbf{k}) & \Delta_{\text{sc}} s_0 \\ -\Delta_{\text{sc}} s_0 & -H_\downarrow(-\mathbf{k}) \end{pmatrix}. \quad (\text{D3})$$

In the curly brace in Eq. (D2), the first term is diamagnetic, while the second term is paramagnetic. $j_x(\mathbf{k}) = (\partial_x H_{\text{BdG}}(\mathbf{k})) \tau_z$ is the electric current operator, where τ_z is the z -component Pauli matrix defined for the Nambu space. Following Ref. [22], one can separate D_s into the conventional and geometric contributions, $D_s = D_s^{\text{conv}} + D_s^{\text{geom}}$. Their expressions are [22]

$$D_s^{\text{conv}} = \frac{1}{4} \sum_{\mathbf{k} \in \text{RBZ}} \sum_{\alpha=\pm} \left[-\frac{\beta}{2 \cosh^2(\beta E_\alpha(\mathbf{k})/2)} + \frac{\tanh(\beta E_\alpha(\mathbf{k})/2)}{E_\alpha(\mathbf{k})} \right] \frac{|\Delta_{\text{sc}}|^2}{E_\alpha(\mathbf{k})^2} \left(\frac{\partial \xi_\alpha(\mathbf{k})}{\partial k_x} \right)^2, \quad (\text{D4})$$

$$D_s^{\text{geom}} = \frac{1}{4} \sum_{\mathbf{k} \in \text{RBZ}} \sum_{\alpha=\pm} \left[\frac{\tanh(\beta E_\alpha(\mathbf{k})/2)}{E_\alpha(\mathbf{k})} - \frac{\tanh(\beta E_{-\alpha}(\mathbf{k})/2)}{E_{-\alpha}(\mathbf{k})} \right] \frac{\xi_{-\alpha}(\mathbf{k}) - \xi_\alpha(\mathbf{k})}{\xi_{-\alpha}(\mathbf{k}) + \xi_\alpha(\mathbf{k})} |\Delta_{\text{sc}}|^2 g_{xx}(\mathbf{k}). \quad (\text{D5})$$

The prefactor 1/4 comes from our different definition of D_s from the one used in Ref. [22]; for the London equation under the Coulomb gauge we use $\mathbf{J} = -4D_s \mathbf{A}$, instead of $\mathbf{J} = -D_s \mathbf{A}$.

In the isolated flat band limit, $D_s^{\text{conv}} \approx 0$. Also, because $\xi_+ \gg \xi_-$ and $E_+ \gg E_-$, the geometric term becomes [22]

$$D_s^{\text{geom}} \approx |\Delta_{\text{sc}}|^2 \sum_{\mathbf{k} \in \text{RBZ}} \frac{\tanh(\beta E_-(\mathbf{k})/2)}{2E_-(\mathbf{k})} g_{xx}(\mathbf{k}). \quad (\text{D6})$$

From $D_s(T)$, we determine the mean field T_{BKT} using the universal relation

$$T_{\text{BKT}} = \frac{\pi}{2} D_s(T_{\text{BKT}}). \quad (\text{D7})$$

APPENDIX E: ADDITIONAL NUMERICAL RESULTS

1. $\mathcal{F} = 0.2$

In Fig. 1 of the main text, we have decomposed our pairing fluctuation theory T_{BKT} into the conventional and geometric contributions. Here we make the same decomposition for the corresponding BCS MF theory T_{BKT} in Fig. 6. Comparing the pairing fluctuation theory and MF results we see that the conventional term in both theories has a dome shape dependence on U with its maximum at $U \sim W$. However, the decrease of the mean field conventional T_{BKT} at large U is much slower and follows a t^2/U asymptote. In contrast, the corresponding pairing fluctuation result falls precipitously to almost zero at $U/t \approx 3$ and remains extremely small at larger U .

The plummet of the pairing fluctuation theory T_{BKT} occurs near the point where μ_F becomes negative. It is associated with a rapid decrease of a term in T_{conv} in Eq. (B21a), (the second one in the square bracket), which is $\propto [\partial_{\xi_\alpha} n_F(\xi_\alpha)](\partial_x \xi_\alpha)^2$. This term vanishes at $T = 0$ when μ_F drops below the band bottom since $[\partial_{\xi_\alpha} n_F(\xi_\alpha)](\partial_x \xi_\alpha)^2 = \delta(\xi_\alpha)(\partial_x \xi_\alpha)^2 \equiv 0$ for any \mathbf{k} . The remaining two terms in Eq. (B21a) cancel each other almost completely at $T = 0$ when μ_F is negative, leading to the extremely small T_{BKT} at $U/t \gtrsim 3$. The near-complete cancellation does not occur when the electron density n is small so that the conduction band is much less than half-filled [17], i.e., when the preformed pairs in the BEC regime are dilute. It suggests that the cancellation is a consequence of a competition between pair hopping and intersite pair repulsion [57], the latter of which originates from Pauli exclusion that prevents two pairs from occupying the same site. The repulsion becomes more important as the density of the pairs, which is equal to $n/2$ in the BEC regime, increases, and it can severely restrict the motion of the pairs at high density [57], leading to almost zero T_{BKT} . This effect of the repulsion

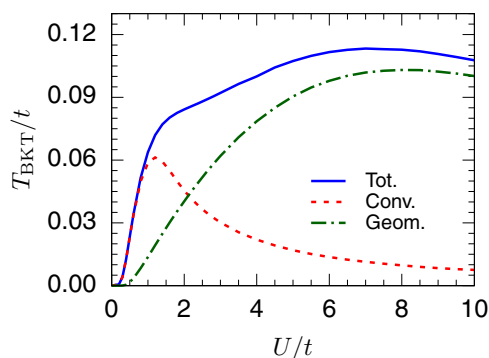


FIG. 6. Decomposition of the BCS MF T_{BKT} into the conventional (“Conv”) and geometric (“Geom”) contributions for the topological $\mathcal{F} = 0.2$ band. $n = 0.3$.

is naturally not included in the calculated mean field D_s , even when the pair density is high and when U is very large [86]. To incorporate the inter-site pair repulsion effect into D_s one needs to include beyond mean field corrections [74,87], in particular quantum fluctuation effects. On the other hand, numerical studies [88–90] on a simple 2D attractive (single-orbital) Hubbard model on a square lattice do not seem to indicate a dramatic effect of the repulsion on T_{BKT} . Of course, the numerical studies can be subject to finite size effects. At present, it is unclear if our calculated conventional n_B/M_B has overestimated the pair repulsion effect or not. Further studies are needed to resolve this issue.

The geometric contribution behaves similarly in the two theories. At small U , it increases roughly linearly with U except where U is very small. At $U/t \gtrsim 7$, it begins to decrease, which comes from a cancellation between the inter- and intraband contributions to T_{geom} in Eq. (B21b). The net result at large enough U is $T_{\text{BKT}}^{\text{geom}} \propto (n_B/M_B)^{\text{geom}} \propto E_g^2/U$, as discussed in Appendix B 4.

2. $\mathcal{F} = 0.01$

Figure 7 illustrates some additional numerical results for the $\mathcal{F} = 0.01$ flat band. In Fig. 7(a), we present a zoomed

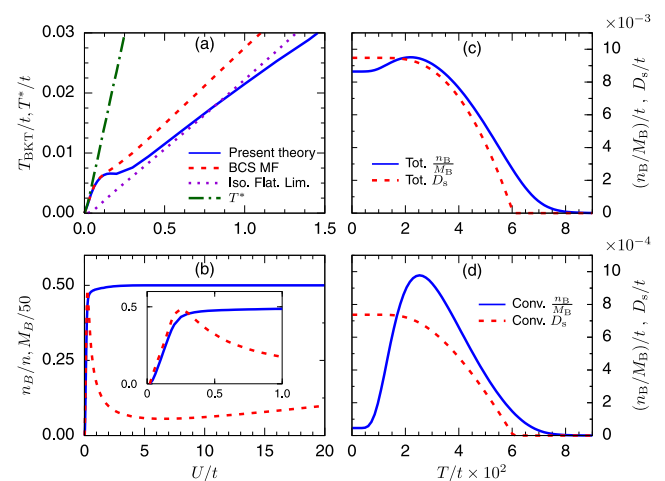


FIG. 7. Results for the topological $\mathcal{F} = 0.01$ band. (a) $\{T_{\text{BKT}}, T^*\}$ and (b) $\{n_B/n, M_B\}$ plotted as a function of U/t . “Iso. Flat. Lim.” stands for the lower bound on T_{BKT} calculated from the lower bound of n_B/M_B in the isolated flat band limit, given by the last line of Eq. (C5). Inset in (b): zoomed view of $\{n_B/n, M_B\}$ at small U/t . M_B is plotted in units of $t a_L^2$, where a_L is the square lattice spacing. [(c) and (d)] n_B/M_B and BCS MF D_s plotted as a function of T/t for $U/t = 0.5$. (c) and (d) show the total and conventional contributions, respectively.

view of the T_{BKT} results at small U . One sees that there is a remnant T_{BKT} peak at $U/t \sim 0.1$, due to the small but still finite conventional contribution to $n_{\text{B}}/M_{\text{B}}$. The latter comes from the fact that the conduction band is not completely flat. From Fig. 7(a), one also sees that the pairing fluctuation theory T_{BKT} almost saturates its lower bound in the isolated flat band limit regime, i.e., at $W \ll U \ll E_{\text{g}}$ where $W \approx 0.035t$ is the lower conduction band width. The near saturation comes from the fact that in the summation of the Berry curvature $\mathcal{F}_{xy}(\mathbf{k})$ in Eq. (C5), $\mathcal{F}_{xy}(\mathbf{k})$ is dominated by one sign with large weight at most \mathbf{k} so that the difference between $\sum_{\mathbf{k}} |\mathcal{F}_{xy}(\mathbf{k})|$ and $|\sum_{\mathbf{k}} \mathcal{F}_{xy}(\mathbf{k})|$ is roughly 10%. This suggests that, if the conduction band were trivial with zero Chern number, the resulting $n_{\text{B}}/M_{\text{B}}$ and T_{BKT} would be reduced by about 90%. Stated alternatively, for a flat band system, nontrivial band topology can significantly boost the two dimensional superconductivity via the quantum metric effect.

Figure 7(b) illustrates that, because of the extremely flat conduction band, even a small attractive interaction $U/t \approx 0.3$ already puts the system in the BEC regime where n_{B}/n saturates to 1/2. Upon entering into the BEC regime, M_{B} exhibits a sharp peak, reflecting the strong localization tendency of the Cooper pairs due to the extremely small conventional contribution to $1/M_{\text{B}}$ in Eq. (B21a). Note that M_{B} plotted in Fig. 7(b) has been rescaled by a factor of 1/50.

In Figs. 7(c) and 7(d), we give a comparison between the total (conventional) $n_{\text{B}}/M_{\text{B}}$ and that of the BCS MF D_s for $U/t = 0.5$. As shown in Fig. 2(b) of the main text, the corresponding geometric contributions to $n_{\text{B}}/M_{\text{B}}$ and D_s are almost identical at low temperatures, even though the corresponding two T_{BKT} are different, as seen from Fig. 7(a). Mathematically,

the near coincidence derives from the fact that the expression for $n_{\text{B}}/M_{\text{B}}$ in this limit, given in Eq. (C4), is identical to that of D_s , given in Eq. (D6), except that the gap parameters Δ in the two are different: $\Delta = \Delta_{\text{pg}}$ in the former while $\Delta = \Delta_{\text{sc}}$ in the latter case. However, at low temperatures, Δ_{pg} and Δ_{sc} in the two approaches (which are based on the same mean field equations) are essentially equal, explaining why $n_{\text{B}}/M_{\text{B}}$ and D_s are nearly the same.

On the other hand, the conventional, as well as the total, contributions to $n_{\text{B}}/M_{\text{B}}$ and D_s behave quite differently. From Fig. 7(c) we see that, in contrast to the monotonic $D_s(T)$, the total $n_{\text{B}}/M_{\text{B}}$ has a small bump at $T \sim T^*/2$, which comes from the small conventional $n_{\text{B}}/M_{\text{B}}$. The latter depends on T nonmonotonically, as shown in Fig. 7(d). Interestingly, similar nonmonotonic behavior has been observed in the phase stiffness of some 2D Josephson-junction arrays where quantum fluctuations play an important role [91,92]. The nonmonotonicity comes from a competition between two physical processes. Near $T = 0$, $(n_{\text{B}}/M_{\text{B}})^{\text{conv}}$ is almost zero, a consequence of the competition between pair hopping and inter-pair repulsion, as explained in Appendix E 1. Increasing T tends to enhance the pair hopping via an ionization process [56], which becomes thermally more accessible. On the other hand, a large temperature also tends to dissociate the Cooper pairs, leading to a decrease of $(n_{\text{B}}/M_{\text{B}})^{\text{conv}}$ as T increases towards T^* . Mathematically, the competition is between different temperature dependencies of n_{B} and $(1/M_{\text{B}})^{\text{conv}}$. The net result is a peak of $(n_{\text{B}}/M_{\text{B}})^{\text{conv}}$ near $T \sim T^*/2$. However, we should note that our results of $n_{\text{B}}/M_{\text{B}}$ become unreliable at $T \sim T^*/2 \gg T_{\text{BKT}}$ where the ‘‘pg approximation’’ breaks down.

-
- [1] Y. Cao, V. Fatemi, A. Demir, S. Fang, S. L. Tomarken, J. Y. Luo, J. D. Sanchez-Yamagishi, K. Watanabe, T. Taniguchi, E. Kaxiras *et al.*, *Nature (London)* **556**, 80 (2018).
 - [2] Y. Cao, V. Fatemi, S. Fang, K. Watanabe, T. Taniguchi, E. Kaxiras, and P. Jarillo-Herrero, *Nature (London)* **556**, 43 (2018).
 - [3] R. Bistritzer and A. H. MacDonald, *Proc. Natl. Acad. Sci. U.S.A.* **108**, 12233 (2011).
 - [4] F. Wu, A. H. MacDonald, and I. Martin, *Phys. Rev. Lett.* **121**, 257001 (2018).
 - [5] J. F. Dodaro, S. A. Kivelson, Y. Schattner, X. Q. Sun, and C. Wang, *Phys. Rev. B* **98**, 075154 (2018).
 - [6] J. Kang and O. Vafek, *Phys. Rev. X* **8**, 031088 (2018).
 - [7] M. Yankowitz, S. Chen, H. Polshyn, Y. Zhang, K. Watanabe, T. Taniguchi, D. Graf, A. F. Young, and C. R. Dean, *Science* **363**, 1059 (2019).
 - [8] N. F. Q. Yuan and L. Fu, *Phys. Rev. B* **98**, 045103 (2018).
 - [9] H. C. Po, L. Zou, A. Vishwanath, and T. Senthil, *Phys. Rev. X* **8**, 031089 (2018).
 - [10] C. Xu and L. Balents, *Phys. Rev. Lett.* **121**, 087001 (2018).
 - [11] B. Roy and V. Jurićić, *Phys. Rev. B* **99**, 121407(R) (2019).
 - [12] H. Isobe, N. F. Q. Yuan, and L. Fu, *Phys. Rev. X* **8**, 041041 (2018).
 - [13] H. C. Po, L. Zou, T. Senthil, and A. Vishwanath, *Phys. Rev. B* **99**, 195455 (2019).
 - [14] G. Tarnopolsky, A. J. Kruchkov, and A. Vishwanath, *Phys. Rev. Lett.* **122**, 106405 (2019).
 - [15] H. S. Arora, R. Polski, Y. Zhang, A. Thomson, Y. Choi, H. Kim, Z. Lin, I. Z. Wilson, X. Xu, J.-H. Chu *et al.*, *Nature (London)* **583**, 379 (2020).
 - [16] Y. J. Uemura, *J. Phys.: Condens. Matter* **16**, S4515 (2004).
 - [17] X. Wang, Q. Chen, and K. Levin, *New J. Phys.* **22**, 063050 (2020).
 - [18] V. Berezinskii, *Sov. Phys. JETP* **34**, 610 (1971).
 - [19] J. M. Kosterlitz and D. J. Thouless, *J. Phys. C* **6**, 1181 (1973).
 - [20] L. Benfatto, C. Castellani, and T. Giamarchi, *Phys. Rev. Lett.* **98**, 117008 (2007).
 - [21] S. Peotta and P. Törmä, *Nat. Commun.* **6**, 8944 (2015).
 - [22] L. Liang, T. I. Vanhala, S. Peotta, T. Siro, A. Harju, and P. Törmä, *Phys. Rev. B* **95**, 024515 (2017).
 - [23] X. Hu, T. Hyart, D. I. Pikulin, and E. Rossi, *Phys. Rev. Lett.* **123**, 237002 (2019).
 - [24] A. Julku, T. J. Peltonen, L. Liang, T. T. Heikkilä, and P. Törmä, *Phys. Rev. B* **101**, 060505(R) (2020).
 - [25] F. Xie, Z. Song, B. Lian, and B. A. Bernevig, *Phys. Rev. Lett.* **124**, 167002 (2020).
 - [26] J. S. Hofmann, E. Berg, and D. Chowdhury, [arXiv:1912.08848](https://arxiv.org/abs/1912.08848).
 - [27] T. Neupert, L. Santos, C. Chamon, and C. Mudry, *Phys. Rev. Lett.* **106**, 236804 (2011).

- [28] L. He, X.-G. Huang, H. Hu, and X.-J. Liu, *Phys. Rev. A* **87**, 053616 (2013).
- [29] J. Zhang, H. Hu, X.-J. Liu, and H. Pu, *Annual Review of Cold Atoms and Molecules* (World Scientific, Singapore, 2014), Chap. 2, pp. 81–143.
- [30] Z. Fu, L. Huang, Z. Meng, P. Wang, X.-J. Liu, H. Pu, H. Hu, and J. Zhang, *Phys. Rev. A* **87**, 053619 (2013).
- [31] Z. Zheng, H. Pu, X. Zou, and G. Guo, *Phys. Rev. A* **90**, 063623 (2014).
- [32] C.-T. Wu, B. M. Anderson, R. Boyack, and K. Levin, *Phys. Rev. B* **91**, 220504(R) (2015).
- [33] A. J. Leggett, in *Modern Trends in the Theory of Condensed Matter* (Springer, Berlin, Heidelberg, 1980), pp. 13–27.
- [34] M. Iskin, *Phys. Rev. A* **97**, 033625 (2018).
- [35] P. Törmä, L. Liang, and S. Peotta, *Phys. Rev. B* **98**, 220511(R) (2018).
- [36] Q. Chen, I. Kosztin, and K. Levin, *Phys. Rev. Lett.* **85**, 2801 (2000).
- [37] N. Marzari and D. Vanderbilt, *Phys. Rev. B* **56**, 12847 (1997).
- [38] N. Marzari, A. A. Mostofi, J. R. Yates, I. Souza, and D. Vanderbilt, *Rev. Mod. Phys.* **84**, 1419 (2012).
- [39] W. Zhao, Q. Wang, M. Liu, W. Zhang, Y. Wang, M. Chen, Y. Guo, K. He, X. Chen, Y. Wang, J. Wang, X. Xie, Q. Niu, L. Wang, X. Ma, J. K. Jain, M. Chan, and Q.-K. Xue, *Solid State Commun.* **165**, 59 (2013).
- [40] See the appendices for details.
- [41] Q. Chen, I. Kosztin, B. Jankó, and K. Levin, *Phys. Rev. Lett.* **81**, 4708 (1998).
- [42] J. Maly, B. Jankó, and K. Levin, *Physica C: Superconductivity* **321**, 113 (1999).
- [43] L. P. Kadanoff and P. C. Martin, *Phys. Rev.* **124**, 670 (1961).
- [44] Q. Chen, J. Stajic, S. Tan, and K. Levin, *Phys. Rep.* **412**, 1 (2005).
- [45] K. Levin, Q. Chen, C.-C. Chien, and Y. He, *Ann. Phys.* **325**, 233 (2010).
- [46] Q. Chen, I. Kosztin, B. Jankó, and K. Levin, *Phys. Rev. B* **59**, 7083 (1999).
- [47] C.-T. Wu, B. M. Anderson, R. Boyack, and K. Levin, *Phys. Rev. Lett.* **115**, 240401 (2015).
- [48] J. P. Provost and G. Vallee, *Commun. Math. Phys.* **76**, 289 (1980).
- [49] M. Tovmasyan, S. Peotta, P. Törmä, and S. D. Huber, *Phys. Rev. B* **94**, 245149 (2016).
- [50] M. G. Ries, A. N. Wenz, G. Zürn, L. Bayha, I. Boettcher, D. Kedar, P. A. Murthy, M. Neidig, T. Lompe, and S. Jochim, *Phys. Rev. Lett.* **114**, 230401 (2015).
- [51] N. Prokof'ev and B. Svistunov, *Phys. Rev. A* **66**, 043608 (2002).
- [52] J. V. Jose, *40 years of Berezinskii-Kosterlitz-Thouless Theory* (World Scientific, Singapore, 2013).
- [53] S. Tung, G. Lamporesi, D. Lobser, L. Xia, and E. A. Cornell, *Phys. Rev. Lett.* **105**, 230408 (2010).
- [54] P. Cladé, C. Ryu, A. Ramanathan, K. Helmerson, and W. D. Phillips, *Phys. Rev. Lett.* **102**, 170401 (2009).
- [55] P. A. Murthy, I. Boettcher, L. Bayha, M. Holzmann, D. Kedar, M. Neidig, M. G. Ries, A. N. Wenz, G. Zürn, and S. Jochim, *Phys. Rev. Lett.* **115**, 010401 (2015).
- [56] P. Nozières and S. Schmitt-Rink, *J. Low Temp. Phys.* **59**, 195 (1985).
- [57] R. Micnas, J. Ranninger, and S. Robaszkiewicz, *Rev. Mod. Phys.* **62**, 113 (1990).
- [58] B. Halperin and D. R. Nelson, *J. Low Temp. Phys.* **36**, 599 (1979).
- [59] K. Epstein, A. M. Goldman, and A. M. Kadin, *Phys. Rev. Lett.* **47**, 534 (1981).
- [60] D. J. Resnick, J. C. Garland, J. T. Boyd, S. Shoemaker, and R. S. Newrock, *Phys. Rev. Lett.* **47**, 1542 (1981).
- [61] A. F. Hebard and A. T. Fiory, *Phys. Rev. Lett.* **50**, 1603 (1983).
- [62] A. T. Fiory, A. F. Hebard, and W. I. Glaberson, *Phys. Rev. B* **28**, 5075 (1983).
- [63] A. M. Kadin, K. Epstein, and A. M. Goldman, *Phys. Rev. B* **27**, 6691 (1983).
- [64] X. Lu, P. Stepanov, W. Yang, M. Xie, M. A. Aamir, I. Das, C. Urgell, K. Watanabe, T. Taniguchi, G. Zhang, A. Bachtold, A. H. MacDonald, and D. K. Efetov, *Nature (London)* **574**, 653 (2019).
- [65] P. Stepanov, I. Das, X. Lu, A. Fahimniya, K. Watanabe, T. Taniguchi, F. H. Koppens, J. Lischner, L. Levitov, and D. K. Efetov, *Nature (London)* **583**, 375 (2020).
- [66] Y. Cao, D. Rodan-Legrain, J. M. Park, F. N. Yuan, K. Watanabe, T. Taniguchi, R. M. Fernandes, L. Fu, and P. Jarillo-Herrero, *arXiv:2004.04148*.
- [67] Y. Saito, J. Ge, K. Watanabe, T. Taniguchi, and A. F. Young, *Nat. Phys.* **16**, 926 (2020).
- [68] X. Liu, Z. Wang, K. Watanabe, T. Taniguchi, O. Vafek, and J. Li, *arXiv:2003.11072*.
- [69] Y. Jiang, X. Lai, K. Watanabe, T. Taniguchi, K. Haule, J. Mao, and E. Y. Andrei, *Nature (London)* **573**, 91 (2019).
- [70] D. Wong, K. P. Nuckolls, M. Oh, B. Lian, Y. Xie, S. Jeon, K. Watanabe, T. Taniguchi, B. A. Bernevig, and A. Yazdani, *Nature (London)* **582**, 198 (2020).
- [71] Y. Xie, B. Lian, B. Jäck, X. Liu, C.-L. Chiu, K. Watanabe, T. Taniguchi, B. A. Bernevig, and A. Yazdani, *Nature (London)* **572**, 101 (2019).
- [72] T. Timusk and B. Statt, *Rep. Prog. Phys.* **62**, 61 (1999).
- [73] M. Iskin, *Phys. Rev. A* **97**, 063625 (2018); **99**, 053603 (2019); **101**, 053631 (2020); *Phys. B: Condens. Matter* **592**, 412260 (2020).
- [74] L. Benfatto, A. Toschi, and S. Caprara, *Phys. Rev. B* **69**, 184510 (2004).
- [75] N. Fukushima, Y. Ohashi, E. Taylor, and A. Griffin, *Phys. Rev. A* **75**, 033609 (2007).
- [76] G. Bighin and L. Salasnich, *Phys. Rev. B* **93**, 014519 (2016).
- [77] L. Zou, H. C. Po, A. Vishwanath, and T. Senthil, *Phys. Rev. B* **98**, 085435 (2018).
- [78] H. C. Po, H. Watanabe, and A. Vishwanath, *Phys. Rev. Lett.* **121**, 126402 (2018).
- [79] J. Ahn, S. Park, and B.-J. Yang, *Phys. Rev. X* **9**, 021013 (2019).
- [80] A. L. Sharpe, E. J. Fox, A. W. Barnard, J. Finney, K. Watanabe, T. Taniguchi, M. A. Kastner, and D. Goldhaber-Gordon, *Science* **365**, 605 (2019).
- [81] M. Serlin, C. L. Tschirhart, H. Polshyn, Y. Zhang, J. Zhu, K. Watanabe, T. Taniguchi, L. Balents, and A. F. Young, *Science* **367**, 900 (2020).

- [82] Y.-H. Zhang, D. Mao, and T. Senthil, *Phys. Rev. Res.* **1**, 033126 (2019).
- [83] N. Bultinck, S. Chatterjee, and M. P. Zaletel, *Phys. Rev. Lett.* **124**, 166601 (2020).
- [84] Q. J. Chen, Ph.D. thesis, University of Chicago, 2000, [arXiv:1801.06266](https://arxiv.org/abs/1801.06266).
- [85] J. Anandan and Y. Aharonov, *Phys. Rev. Lett.* **65**, 1697 (1990).
- [86] P. J. H. Denteneer, G. An, and J. M. J. van Leeuwen, *Phys. Rev. B* **47**, 6256 (1993).
- [87] N. Dupuis, *Phys. Rev. B* **70**, 134502 (2004).
- [88] M. Keller, W. Metzner, and U. Schollwöck, *Phys. Rev. Lett.* **86**, 4612 (2001).
- [89] A. Toschi, P. Barone, M. Capone, and C. Castellani, *New J. Phys.* **7**, 7 (2005).
- [90] T. Paiva, R. Scalettar, M. Randeria, and N. Trivedi, *Phys. Rev. Lett.* **104**, 066406 (2010).
- [91] C. Rojas and J. V. José, *Phys. Rev. B* **54**, 12361 (1996).
- [92] L. Capriotti, A. Cuccoli, A. Fubini, V. Tognetti, and R. Vaia, *Phys. Rev. Lett.* **91**, 247004 (2003).